Electronic Journal of Differential Equations, Vol. 2011 (2011), No. 132, pp. 1–30.
ISSN: 1072-6691. URL: http://ejde.math.txstate.edu or http://ejde.math.unt.edu
ftp ejde.math.txstate.edu (login: ftp)

NUMERICAL INVESTIGATION OF THE SMALLEST EIGENVALUES OF THE p-LAPLACE OPERATOR ON PLANAR DOMAINS

JIŘÍ HORÁK

Abstract. The eigenvalue problem for the p-Laplace operator with $p > 1$ on planar domains with zero Dirichlet boundary condition is considered. The Constrained Descent Method and the Constrained Mountain Pass Algorithm are used in the Sobolev space setting to numerically investigate the dependence of the two smallest eigenvalues on p. Computations are conducted for values of p between 1.1 and 10. Symmetry properties of the second eigenfunction are also examined numerically. While for the disk an odd symmetry about the nodal line dividing the disk in halves is maintained for all the considered values of p, for rectangles and triangles symmetry changes as p varies. Based on the numerical evidence the change of symmetry in this case occurs at a certain value p_0 which depends on the domain.

1. Introduction

For a bounded domain $\Omega \subset \mathbb{R}^N$, $N \in \mathbb{N}$ and a parameter $p \in (1, \infty)$ consider the nonlinear eigenvalue problem

$$\begin{aligned} -\Delta_p u &= \lambda |u|^{p-2} u \quad \text{in } \Omega, \\ u &= 0 \quad \text{on } \partial\Omega \end{aligned} \tag{1.1}$$

to be solved for a real function $u : \Omega \to \mathbb{R}$ and a parameter $\lambda \in \mathbb{R}$. The operator $\Delta_p u := \operatorname{div}\left(|\nabla u|^{p-2}\nabla u\right)$ is called the p-Laplace operator. If for a certain λ a nontrivial weak solution $u \in W_0^{1,p}(\Omega)$ of (1.1) exists, we call λ and u Dirichlet eigenvalue and eigenfunction of the p-Laplace operator, respectively. Problem (1.1) is homogeneous but in general not additive in u.

From [1, 20, 21, 4] and others it is well known that there exists a smallest eigenvalue λ_1 and that it is positive, isolated and simple (i.e., the corresponding eigenfunction u_1 is unique up to multiplication by a constant). Moreover, for any eigenfunction u it holds: u corresponds to λ_1 if and only if it does not change its sign on Ω. In [12] the authors constructed a nondecreasing sequence of eigenvalues accumulating at infinity using a variational approach. Since between λ_1 and the next member of this sequence there are no other eigenvalues, as it was shown in [2], we call this second smallest eigenvalue λ_2 and a corresponding eigenfunction

2000 *Mathematics Subject Classification.* 35J92, 49M30, 49R05.
Key words and phrases. p-Laplace operator; eigenvalue; mountain pass algorithm; symmetry.

Submitted September 22, 2011. Published October 13, 2011.

u_2. In general, however, it is not known yet whether this sequence contains all the eigenvalues. Nodal domains of variational eigenfunctions were studied in [11]. The regularity results of [10] imply that any eigenfunction (perhaps redefined on a class of measure zero) is of class $C^{1,\alpha}(\Omega)$ for some $\alpha > 0$.

An early attempt at computing several eigenpairs of the p-Laplace operator on a planar domain ($N = 2$) numerically is due to Brown and Reichel [7]. Under the assumption of radial symmetry they used a shooting method for the resulting ordinary differential equation. The first genuinely two-dimensional approach was taken by Yao and Zhou [24] using their local minimax method based on a variational formulation. For a square $\Omega = \{(x_1, x_2) : x_1, x_2 \in (0, 2)\}$ and $p \in \{1.75, 2.5, 3.0\}$ the authors computed approximations to seven eigenvalues and corresponding eigenfunctions. They observed that the found eigenfunction u_2 has an odd symmetry about $x_1 = 1$ for $p < 2$ and about $x_1 = x_2$ for $p > 2$.

The goal of the current work is to apply the numerical variational methods of [14] to compute approximations of the two smallest eigenvalues and to visualize the corresponding eigenfunctions on a planar domain. In particular the focus is

- to extend the Constrained Mountain Pass Algorithm from the Hilbert space setting (as described in [8] and [14]) to the Banach space $W_0^{1,p}(\Omega)$; to verify that this algorithm is suitable even for computations with p "far" from 2;
- to observe the behavior of the eigenpairs for a large range of p and compare it with the known theoretical results about the asymptotics for $p \to 1$ and $p \to \infty$;
- to observe changes in symmetry of u_2 on various domains.

In Section 2 we review known results about the variational properties of λ_1 and λ_2 and their asymptotic behavior. The variational numerical methods applied to compute the eigenpairs are summarized in Sec. 3. The choice of a descent direction in the Banach space $W_0^{1,p}(\Omega)$ is discussed in detail here, too. In Sec. 4 we present the numerical results for several planar domains. We pay a particular attention to the dependence of the eigenvalues on p and changes of symmetry of the second eigenfunction. Several issues concerning the application of the numerical methods (like mesh refinement, choice of parameters, etc.) are addressed in Sec. 5. Finally, Sec. 6 summarizes our numerical observations and the Appendix provides proofs of claims used in Sec. 3.

2. Background material

In the Introduction we mentioned the existence of the first two eigenvalues λ_1 and λ_2. Now we review some known results about their variational characterization based on the above references and their asymptotic behavior for p close to 1 and p large.

2.1. Variational characterization of λ_1 and λ_2.

Define two continuously Fréchet differentiable functionals $I, J \in C^1\big(W_0^{1,p}(\Omega), \mathbb{R}\big)$:

$$I(u) := \int_\Omega |\nabla u|^p \, dx, \quad J(u) := \int_\Omega |u|^p \, dx. \tag{2.1}$$

Their Fréchet derivatives $I'(u), J'(u)$ are members of the dual space of $W_0^{1,p}(\Omega)$ which we denote by $W^{-1,q}(\Omega)$, where $\frac{1}{p}+\frac{1}{q}=1$, and are given by

$$\langle I'(u),\phi\rangle = p\int_\Omega |\nabla u|^{p-2}\nabla u\nabla\phi\,dx, \quad \langle J'(u),\phi\rangle = p\int_\Omega |u|^{p-2}u\phi\,dx. \tag{2.2}$$

Two observation can be made: 1. After testing (1.1) with $\phi\in W_0^{1,p}(\Omega)$ and integrating by parts it becomes clear that (1.1) is the Euler-Lagrange equation $I'(u)-\lambda J'(u)=0$ (up to the factor p) which all critical points of I with respect to the constraint

$$S := \big\{u\in W_0^{1,p}(\Omega) : J(u)=1\big\} \tag{2.3}$$

must satisfy for some value of the Lagrange multiplier λ.

2. If (λ,u) is an eigenpair and we test (1.1) with u, we obtain the Rayleigh quotient

$$\lambda = \frac{\int_\Omega |\nabla u|^p\,dx}{\int_\Omega |u|^p\,dx}. \tag{2.4}$$

Since both its numerator and denominator are homogeneous of the same degree in u, finding the smallest eigenvalue λ is the same as minimizing I on S:

$$\lambda_1 = \min_{u\in S} I(u). \tag{2.5}$$

A variational minimax characterization of the second eigenvalue λ_2 based on the Krasnoselskii genus was given in [12]. Alternatively, since for $u_1\in S$ both u_1 and $-u_1$ are local minimizers of I on S, a mountain pass characterization of λ_2 is also possible [9]:

$$\lambda_2 = \inf_{\gamma\in\Gamma}\max_{u\in\gamma([0,1])} I(u), \tag{2.6}$$

where $\Gamma=\{\gamma\in C([0,1],S) : \gamma(0)=u_1,\ \gamma(1)=-u_1\}$ is the family of all paths in S connecting the two local minimizers. Hence for the numerical computations we have the setting required by the Constrained Mountain Pass Algorithm of [14].

2.2. **Asymptotic behavior of λ_1 and λ_2 as $p\to 1$.** To make the dependence of an eigenvalue on the domain Ω and the parameter p explicit in our notation we will write $\lambda(\Omega;p)$ if necessary (and similarly for eigenfunctions). The main result of [17] implies that for Ω with a Lipschitz boundary

$$\lim_{p\to 1}\lambda_1(\Omega;p) = h_1(\Omega), \quad \text{where } h_1(\Omega) := \min_{D\subset\Omega}\frac{\mathrm{Per}(D)}{|D|} \tag{2.7}$$

is called Cheeger constant, $\mathrm{Per}(D)$ denotes the perimeter of D measured with respect to $\mathbb{R}^N$ and $|D|$ its N-dimensional Lebesgue measure. A minimizing set in the definition of $h_1(\Omega)$ is called a Cheeger set of Ω. Furthermore, any convex planar domain Ω possesses a unique Cheeger set $\mathcal{C}_\Omega$ and

$$\lim_{p\to 1} u_1(\Omega;p) = \chi_{\mathcal{C}_\Omega} \quad \text{in } L^1 \text{ along a subsequence.} \tag{2.8}$$

Here the eigenfunctions $u_1(\Omega;p)$ have been normalized to 1 in the L^∞-norm, $\chi_{\mathcal{C}_\Omega}$ is the indicator function of $\mathcal{C}_\Omega$.

A detailed description of how to find the Cheeger set $\mathcal{C}_\Omega$ for a convex planar domain Ω is given in [18]. Its main property is

$$\mathcal{C}_\Omega = \cup\{B\subset\Omega : B \text{ is a ball of radius } \tfrac{1}{h_1(\Omega)}\}. \tag{2.9}$$

In [22] it was shown that for Ω with a Lipschitz boundary it holds:

$$\lim_{p\to 1} \lambda_2(\Omega;p) = h_2(\Omega), \tag{2.10}$$

where

$$h_2(\Omega) := \min\{\mu \in \mathbb{R} : \exists D_1, D_2 \subset \Omega, D_1 \cap D_2 = \emptyset \text{ and } \max_{i=1,2} \frac{\mathrm{Per}(D_i)}{|D_i|} \le \mu\} \tag{2.11}$$

is called the second Cheeger constant and the convention $\mathrm{Per}(D)/|D| = \infty$ is used if $|D| = 0$. Any two sets D_1, D_2 for which the minimum in the definition of $h_2(\Omega)$ is achieved are called coupled Cheeger sets of Ω. For a result about the L^1-convergence of the second eigenfunctions we refer to [22, Thm. 5.11].

2.3. **Asymptotic behavior of λ_1 and λ_2 as $p \to \infty$.** For a bounded domain Ω of $\mathbb{R}^N$ a limit problem of (1.1) as $p \to \infty$ is studied in [16, 15] for an unknown function u and an unknown real parameter Λ (see [15, Definition 2.1]). The smallest Λ for which this limit problem admits a nontrivial viscosity solution is called the first ∞-eigenvalue and denoted Λ_1. For Λ_1 there exists a positive viscosity solution and it holds:

$$\lim_{p\to\infty} \big(\lambda_1(\Omega;p)\big)^{1/p} = \Lambda_1(\Omega), \tag{2.12}$$

$$\Lambda_1(\Omega) = \frac{1}{r_1}, \quad \text{where } r_1 := \sup\{r > 0 : \exists \text{ an open ball } B \subset \Omega \text{ of radius } r\}, \tag{2.13}$$

$$\Lambda_1(\Omega) = \min\Big\{\frac{\|\nabla u\|_{L^\infty(\Omega)}}{\|u\|_{L^\infty(\Omega)}} : u \in W_0^{1,\infty}(\Omega) \setminus \{0\}\Big\}. \tag{2.14}$$

The characterization (2.14) is an analogy of (2.4) and (2.5). Furthermore, for any sequence $\{u_1(\Omega;p_i)\}_{i=1}^\infty$ with $p_i \to \infty$ and $\|u_1(\Omega;p_i)\|_{L^{p_i}(\Omega)} = 1$ there exists a subsequence converging uniformly to a viscosity solution of the limit problem for $\Lambda_1(\Omega)$.

The smallest Λ for which the limit problem admits a viscosity solution with at least two nodal domains is called the second ∞-eigenvalue and denoted Λ_2. From the definition it follows that $\Lambda_1 \le \Lambda_2$. If this inequality is strict, then zero is the only solution of the limit problem for $\Lambda \in (\Lambda_1, \Lambda_2)$. It holds:

$$\lim_{p\to\infty} \big(\lambda_2(\Omega;p)\big)^{1/p} = \Lambda_2(\Omega), \tag{2.15}$$

$$\Lambda_2(\Omega) = \frac{1}{r_2}, \tag{2.16}$$

where $r_2 := \sup\{r > 0 : \exists \text{ disjoint open balls } B_1, B_2 \subset \Omega \text{ of radius } r\}$,

$$\Lambda_2(\Omega) = \inf_{\gamma\in\Gamma} \max_{u\in\gamma([0,1])} \|\nabla u\|_{L^\infty(\Omega)}, \tag{2.17}$$

where Γ is defined as in (2.6), u_1 is any first ∞-eigenfunction and $S := \{u \in W_0^{1,\infty}(\Omega) : \|u\|_{L^\infty(\Omega)} = 1\}$. Furthermore, for any sequence $\{u_2(\Omega;p_i)\}_{i=1}^\infty$ with $p_i \to \infty$ and $\|u_2(\Omega;p_i)\|_{L^{p_i}(\Omega)} = 1$ there exists a subsequence converging uniformly to a viscosity solution of the limit problem for $\Lambda_2(\Omega)$ which has at least two nodal domains.

3. Numerical methods

An overview of the numerical methods used to compute approximations of the first and the second Dirichlet eigenpair of the p-Laplace operator is given in Fig. 1. In this section we will describe these methods. Our goal is to find u_1 as a minimizer of I on S according to (2.5) and u_2 as a mountain pass point of I on S according to (2.6). We first discretize the planar domain Ω using a mesh of triangles and apply the finite element method to approximate $W_0^{1,p}(\Omega)$ by a finite dimensional subspace. Then we fix $p \in (1,\infty)$ and use a variant of the *Constrained Steepest Descent Method* (CDM) to find the first eigenpair, and the *Constrained Mountain Pass Algorithm* (CMPA) to find the second eigenpair. We implement both methods based on [14]. There are, however, several important issues arising from the fact that we work in a Banach space and not a Hilbert space as in [14]. How to deal with these issues will also be explained in this section. For the computation of the descent direction the Augmented Lagrangian Method of [13] is applied.

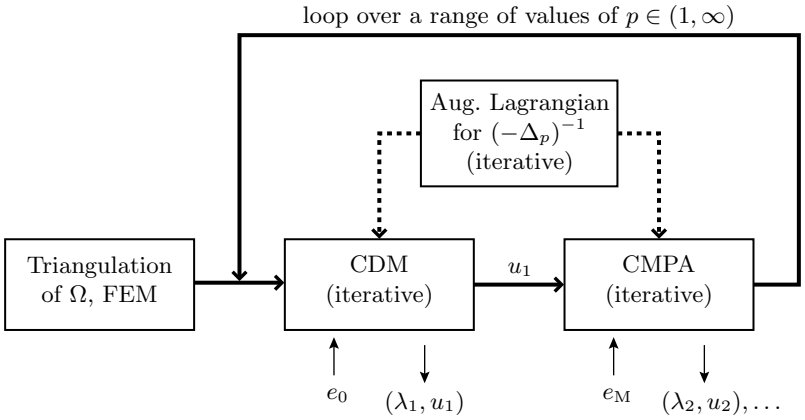

Figure 1. Flowchart of the numerical computations.

3.1. **Finite element method.** A finite element approximation of the p-Laplacian was studied in [3]. We adopt this approach for our computations. The planar domain Ω is approximated by a polygonal domain Ω^h which is partitioned into a finite number of triangles of diameter at most h. Let $\{a_i\}_{i=1}^k$ be the set of those triangle vertices which lie in the interior of Ω^h. Functions $\{\phi_i\}_{i=1}^k$ forming a basis of the k-dimensional subspace V_0^h of $W_0^{1,p}(\Omega^h)$ are chosen linear on each triangle with $\phi_i(a_j) = \delta_{ij}$, where δ_{ij} is the Kronecker delta, and zero on $\partial\Omega^h$. The space V_0^h is our finite element approximation of the Sobolev space $W_0^{1,p}(\Omega)$.

In [3] a detailed description of this method was given for the boundary value problem

$$\begin{aligned} -\Delta_p u &= f \quad \text{in } \Omega, \\ u &= 0 \quad \text{on } \partial\Omega \end{aligned} \tag{3.1}$$

with the right-hand side $f \in L^2(\Omega)$. Since it is a straightforward task to adapt it to our problem (1.1) with $\lambda|u|^{p-2}u$ on the right-hand side, we will not show the details here.

We will however mention one additional technical detail involved. The evaluation of the functionals given in (2.1) and (2.2) for functions from V_0^h amounts to adding up the contributions of the individual triangles that make up Ω^h. For example, for $I(u)$ with $u \in V_0^h$ one merely needs to integrate a constant on every triangle. The situation is different for $J(u)$. Let $T \subset \Omega^h$ be a triangle with area $|T|$ and vertices A, B, and C and let u be a linear function on T with values u_A, u_B, and u_C at these vertices, respectively. If these values are mutually different, then the following formula holds:

$$\begin{aligned}\int_T |u|^p\,dx = &\frac{2\,|T|}{(p+1)(p+2)(u_C-u_A)}\\ &\times\Big(\frac{|u_C|^{p+2}-|u_B|^{p+2}}{u_C-u_B}-\frac{|u_A|^{p+2}-|u_B|^{p+2}}{u_A-u_B}\Big).\end{aligned} \tag{3.2}$$

By inspecting this formula we see that great care must be taken when implementing it to avoid numerical cancellations. This is crucial for the success of our method. A similar situation occurs when evaluating $\langle J'(u),\phi\rangle$ (or the right-hand side of the equation in (1.1) in the weak formulation).

3.2. **Direction of descent.** An important ingredient of the variational numerical methods CDM and CMPA is finding a descent direction of the functional I on the constraint set S. How this is accomplished in the Hilbert space setting was shown in [14]: Let $\nabla I(u)$ be the Riesz representation of $I'(u)$ (i.e., the gradient) and P_u the orthogonal projection on the tangent space of S at $u \in S$. Then

$$w_u = -P_u \nabla I(u), \quad u \in S \tag{3.3}$$

gives the steepest descent direction of I at u with respect to S.

Because of the lack of orthogonality in the Banach space $W_0^{1,p}(\Omega)$ we need to take a different approach. Let

$$T_uS := \big\{v \in W_0^{1,p}(\Omega) : \langle J'(u), v\rangle = 0\big\}, \quad \|v\| := \Big(\int_\Omega |\nabla v|^p\,dx\Big)^{1/p} \tag{3.4}$$

denote the tangent space of S at $u \in S$ and the norm of $v \in W_0^{1,p}(\Omega)$, respectively. The problem of finding the steepest descent direction of I with respect to S can be written as follows: for a given $u \in S$ which is not a critical point of I with respect to S

$$\text{minimize } \langle I'(u), w\rangle \quad \text{subject to} \quad w \in \{v \in T_uS : \|v\| = 1\}. \tag{3.5}$$

The existence of a unique solution can be proved in a straightforward way using a minimizing sequence (in a reflexive Banach space, in general). This solution must satisfy the Euler-Lagrange equation

$$-\Delta_p w = \beta\left(-\Delta_p u - \alpha|u|^{p-2}u\right), \tag{3.6}$$

where $\alpha, \beta \in \mathbb{R}$ are unknown. The coefficient β comes from the requirement $\|w\| = 1$. After testing (3.6) by w it can be seen that $\beta < 0$ since the minimum in (3.5) is negative. For $p \neq 2$ finding the right α is not an easy problem.

We will try to find a different convenient descent direction instead, not necessarily the steepest one. A simple calculation shows that under no constraints the steepest descent direction of I at $u \in W_0^{1,p}(\Omega)$ is given by $-u$. For $u \in S$ we consider the point $w_u \in T_uS$ closest to $-u$, i.e., the unique solution of the minimization problem

$$\text{minimize } \|w+u\| \quad \text{subject to} \quad w \in T_uS. \tag{3.7}$$

The minimizer must satisfy the Euler-Lagrange equation

$$-\Delta_p(w+u) = \alpha|u|^{p-2}u \tag{3.8}$$

for some $\alpha \in \mathbb{R}$. Unlike (3.6), this equation can be solved easily for w:

$$w_u = -u + \frac{1}{\int_\Omega |u|^{p-2}u\, v_u\, dx}\, v_u, \quad \text{where } v_u := (-\Delta_p)^{-1}\left(|u|^{p-2}u\right). \tag{3.9}$$

The operator $(-\Delta_p)^{-1}$ is discussed later in Sec. 3.3. Lemma 7.1 in the Appendix shows that w_u is, indeed, a descent direction of I with respect to S. This descent direction is used in our implementation of the variational numerical methods CDM and CMPA.

Remark 3.1. 1. Observe that if $-\Delta_p$ were linear, equations (3.6) and (3.8) would coincide (after setting $\beta = -1$). Hence in case $p = 2$ they yield the same descent direction (which is the one given by (3.3)).

2. With $\beta = -1$ in (3.6), both equations (3.6) and (3.8) yield a zero solution if and only if u is a critical point of I with respect to S.

3.3. **Inverse of the p-Laplace operator.** A classical result (see, e.g., [23, Theorem 1.3]) says that for any $f \in W^{-1,q}(\Omega)$, the dual of $W_0^{1,p}(\Omega)$ with $\frac{1}{p} + \frac{1}{q} = 1$, the problem

$$\begin{aligned} -\Delta_p u &= f \quad \text{in } \Omega, \\ u &= 0 \quad \text{on } \partial\Omega \end{aligned} \tag{3.10}$$

has a unique weak solution in $W_0^{1,p}(\Omega)$. This means that the operator

$$-\Delta_p : W_0^{1,p}(\Omega) \to W^{-1,q}(\Omega) \quad \text{given by} \quad \langle -\Delta_p u, v\rangle = \int_\Omega |\nabla u|^{p-2}\nabla u \nabla v\, dx \tag{3.11}$$

is invertible. We denote its inverse by $(-\Delta_p)^{-1}$.

In order to use the descent direction given by (3.9) we need to compute v_u first, i.e., we need to solve problem (3.10) numerically. For that we apply the Augmented Lagrangian Method of [13]. Here we give a brief description of this method. Let V_0^h be again the subspace of continuous functions of $W_0^{1,p}(\Omega^h)$ which are linear on every triangle of a triangulation of Ω^h, D^h the space of functions with values in $\mathbb{R}^2$ defined on Ω^h which are constant on each triangle, and $r > 0$ a parameter. For the Augmented Lagrangian

$$\mathcal{L}_r(v,t,\mu) := \frac{1}{p}\int_\Omega |t|^p\, dx - \langle f, v\rangle + \frac{r}{2}\int_\Omega |\nabla v - t|^2\, dx + \int_\Omega \mu\cdot(\nabla v - t)\, dx, \tag{3.12}$$

where $v \in V_0^h$ and $t, \mu \in D^h$, a saddle point (u, s, η) is searched for such that

$$\mathcal{L}_r(u,s,\mu) \le \mathcal{L}_r(u,s,\eta) \le \mathcal{L}_r(v,t,\eta) \quad \forall (v,t,\mu) \in V_0^h \times D^h \times D^h. \tag{3.13}$$

A sequence $\left(u^{(n)}, s^{(n)}, \eta^{(n)}\right)$ approximating (u, s, η) is constructed as follows: choose $\left(s^{(0)}, \eta^{(1)}\right) \in D^h \times D^h$ and for $n \in \mathbb{N}$ solve

$$\begin{aligned} -r\Delta u^{(n)} &= f + \eta^{(n)}\cdot\nabla - r\, s^{(n-1)}\cdot\nabla \quad \text{in } \Omega, \\ u^{(n)} &= 0 \quad \text{on } \partial\Omega, \end{aligned} \tag{3.14}$$

$$\left|s^{(n)}\right|^{p-2}s^{(n)} + r\, s^{(n)} = r\nabla u^{(n)} + \eta^{(n)}, \tag{3.15}$$

$$\eta^{(n+1)} = \eta^{(n)} + r\left(\nabla u^{(n)} - s^{(n)}\right). \tag{3.16}$$

For given $s^{(n-1)}$ and $\eta^{(n)}$ the boundary value problem (3.14) can be solved for $u^{(n)}$. For this, one just needs some standard algorithm for finding the inverse of the Laplace operator with Dirichlet boundary conditions. The equation in (3.14) is understood in the weak sense: for example, the term $\eta^{(n)} \cdot \nabla$ is evaluated as $\int_\Omega \eta^{(n)} \cdot \nabla\phi \, dx$ for a test function $\phi \in V_0^h$.

Next, equation (3.15) is used to find $s^{(n)}$. The $\mathbb{R}^2$-norm of $s^{(n)}$ must satisfy

$$\left|s^{(n)}\right|^{p-1} + r\left|s^{(n)}\right| = \left|r\,\nabla u^{(n)} + \eta^{(n)}\right|, \tag{3.17}$$

which on each triangle is just a scalar nonlinear equation with one unknown. For each triangle it can be solved, e.g., by Newton's method. After $|s^{(n)}|$ has been obtained, $s^{(n)}$ can be computed immediately from (3.15).

At the end η is updated according to (3.16) and a new iteration step can be started. The convergence of this method was studied in [13]. We use the norm of $\nabla u^{(n)} - s^{(n)}$ to measure the convergence.

3.4. **Constrained Descent Method.** The Constrained Descent Method (CDM) is applied to find the first eigenpair of the p-Laplace operator: u_1 is found as the minimizer of I with respect to S, $\lambda_1 = I(u_1)$. As mentioned above, it differs from the Constrained Steepest Descent Methods of [14] in the way the descent direction is chosen.

The method solves numerically the initial value problem

$$\frac{d}{dt}u(t) = w_{u(t)}, \quad u(0) = e_0 \in S, \tag{3.18}$$

where w_u is given by (3.9) for $u \in S$. Proposition 7.3 in the Appendix states that this problem has a unique solution $u(t) \in S$ for $t \in (0,\infty)$ and that $u(t)$ gets arbitrarily close to a critical point of I with respect to S as $t \to \infty$.

After choosing the starting point $e_0 \in S$ and setting $u^{(0)} := e_0$ the initial value problem is solved by repeating the following two steps: First (Euler's step), given $u^{(n-1)}$ find $\bar{u}^{(n)} = u^{(n-1)} + \Delta t^{(n)}\, w_{u^{(n-1)}}$ with some small value $\Delta t^{(n)} > 0$. Second (scaling), define $u^{(n)} = c\bar{u}^{(n)}$, where the coefficient $c \in \mathbb{R}$ is chosen such that $u^{(n)} \in S$. In case $I\big(u^{(n)}\big) > I\big(u^{(n-1)}\big)$, halve the step $\Delta t^{(n)}$ and compute $\bar{u}^{(n)}$ and $u^{(n)}$ again. If this halving has to be repeated and $\Delta t^{(n)}$ becomes very small (smaller than a prescribed threshold value), stop the algorithm. The norm of the descent direction $\|w_{u^{(n-1)}}\|$ is used to measure convergence of $u^{(n)}$ to an eigenfunction u. When computing w_u according to (3.9) the integral $\nu := \int_\Omega |u|^{p-2}u\, v_u \, dx$ has to be evaluated. If $\|w_{u^{(n-1)}}\|$ is small, then $\big(1/\nu^{(n-1)}\big)^{p-1}$ approximates the eigenvalue.

We note that at every step of CDM the Augmented Lagrangian Method of Sec. 3.3 has to be applied to compute the descent direction $w_{u^{(n-1)}}$.

3.5. **Constrained Mountain Pass Algorithm.** Suppose that an approximation of the first eigenvalue λ_1 and eigenfunction u_1 of the p-Laplace operator have been computed. Constrained Mountain Pass Algorithm (CMPA) is applied to find the second eigenpair: u_2 is found as a mountain pass point of I on S lying "between" the two local minimizers u_1 and $-u_1$, $\lambda_2 = I(u_2)$. Again, it differs from CMPA described in detail in [14] in the choice of the descent direction.

We give a short summary here based on the original description of the Mountain Pass Algorithm by Choi and McKenna [8]: Take a discretized path $\{z_j\}_{j=0}^P \subset S$ connecting $z_0 := u_1$ with $z_P := -u_1$. After finding the path point $z_m =: z^{\max}$ at

which I is maximal along the path, move this point a small distance in the tangent space to S at $z^{\max}$ in the descent direction $w_{z^{\max}}$ and then scale it (as in CDM) to come back to S. Thus the path has been deformed on S and the maximum of I lowered. Repeat this deforming of the path until the maximum along the path cannot be lowered anymore: a mountain pass point of I with respect to S has been reached.

To construct the initial path connecting u_1 and $-u_1$ in S we choose an intermediate point $e_{\mathrm{M}} \in S \setminus \{\pm u_1\}$, set $k := [P/2]$ and define:

$$\begin{aligned}
\bar{z}_j &:= u_1 + \frac{j}{k}(e_{\mathrm{M}} - u_1) \quad \text{for } j \in \{0, \dots, k\},\\
\bar{z}_j &:= e_{\mathrm{M}} + \frac{j-k}{P-k}(-u_1 - e_{\mathrm{M}}) \quad \text{for } j \in \{k, \dots, P\},\\
z_j &:= c_j \bar{z}_j \in S \text{ (scaling to } S \text{ as in Sec. 3.4)} \quad \text{for } j \in \{0, \dots, P\}.
\end{aligned}$$

Connecting u_1 and $-u_1$ by a line segment without the intermediate point e_{M} would not work. Such a line segment passes through 0 and cannot be scaled to get to S.

Finally, as in CDM, $\|w_{z^{\max}}\|$ is used to measure convergence to an eigenfunction u. The corresponding eigenvalue λ is computed as in CDM, too. At every step of CMPA the Augmented Lagrangian Method of Sec. 3.3 has to be applied to compute the descent direction $w_{z^{\max}}$.

4. Numerical results

In this section numerical results will be given for the following planar domains: the unit disk, the square with side length 2, the rectangle with sides 2 and 7/4, the isosceles triangle with base and height 1, the isosceles triangle with base 1 and height 3/4, and the equilateral triangle with side 1. Unless explicitly stated otherwise the computed eigenfunctions will be plotted as a surface over the domain with heights given by the function values and as a contour plot of these values (like, e.g., in Fig. 2). In order to better compare the shapes, the eigenfunctions in these figures have been scaled to have the same maximum value. We do not explicitly differentiate between two eigenfunctions u and $\tilde{u}$ if $\tilde{u}(x) = cu(Tx)$, where $c \in \mathbb{R}$ is a scaling coefficient and $T : \Omega \to \Omega$ is some symmetry transformation of Ω (e.g., for a square a rotation by $\pi/2$ about the center of the square).

Animated graphs of the computed eigenfunctions u_1 and u_2 for the considered domains are available as an electronic data supplement to this paper from author's home page and using pointers on the journal's web page.

4.1. **Unit Disk.** Let

$$\Omega := \left\{(x_1, x_2) \in \mathbb{R}^2 : x_1^2 + x_2^2 < 1\right\}.$$

Before presenting the numerical results we make a remark about the radially symmetric case. It is known that the first eigenfunction for the disk is radially symmetric. One important question about the second eigenfunction for the disk has been whether it is radially symmetric, too. In [22, 5] the authors proved that for p close to 1 the answer is no. The eigenvalue problem (1.1) under the assumption of radial symmetry $u = u(r)$, $r \in (0, 1)$ becomes

$$\begin{aligned}
-\left(r|u'|^{p-2}u'\right)' &= \lambda r|u|^{p-2}u,\\
u'(0) = 0, \quad u(1) &= 0.
\end{aligned} \tag{4.1}$$

This and a related problem are treated, for example, in [7] and [5], where numerical approaches play an important role. For the current numerical investigation we adapt our *genuine 2D method* described in Sec. 3 in the following ways:

- all integrals are one-dimensional,
- the weight r is introduced,
- the natural boundary condition is implemented at $r = 0$ (the zero boundary condition stays at $r = 1$).

Since these modifications are rather elementary, we will not describe them in more detail. We will refer to this method as *radial 2D method*.

For the computations carried out by the genuine 2D method the domain Ω was approximated by a polygon and discretized using 68,608 triangles. For the computations carried out by the radial 2D method the interval $(0, 1)$ was divided into 1,000 subintervals of the same length.

(a)

p	λ_1	λ_2	λ_2^{rad}
1.1	2.5690	4.2008	5.6809
1.2	2.9654	5.0707	7.2277
1.3	3.3263	5.9604	8.9302
1.4	3.6740	6.9072	10.861
1.5	4.0179	7.9310	
1.6	4.3623	9.0465	
1.7	4.7097	10.266	
1.8	5.0618	11.604	
1.9	5.4194	13.072	
2.0	5.7834	14.683	
2.1	6.1542	16.452	
2.2	6.5320	18.395	
2.3	6.9173	20.527	
2.4	7.3102	22.866	
2.5	7.7107	25.432	
3.0	9.8323	42.460	
4.0	14.683	110.71	
5.0	20.351	273.00	
6.0	26.832	649.47	
8.0	42.210	3,430.1	
10.0	60.784	17,071	

(b)

p	λ_1	λ_2^{rad}
1.1	2.5688	5.6762
1.2	2.9653	7.2251
1.3	3.3260	8.9279
1.4	3.6739	10.858
1.5	4.0177	13.073
1.6	4.3621	15.626
1.7	4.7095	18.574
1.8	5.0616	21.982
1.9	5.4192	25.921
2.0	5.7831	30.471
2.1	6.1539	35.725
2.2	6.5317	41.788
2.3	6.9169	48.780
2.4	7.3097	56.836
2.5	7.7102	66.112
3.0	9.8314	137.93
4.0	14.681	559.02
5.0	20.347	2,132.7
6.0	26.823	7,822.6
8.0	42.182	97,462
10.0	60.715	$1.1359 \cdot 10^6$

TABLE 1. Eigenvalues for the disk computed numerically by: (a) the genuine 2D method, (b) the radial 2D method.

Figure 2 shows the eigenfunction u_2 computed by the genuine 2D method for several values of p. The computed eigenvalues λ_1 and λ_2 for these and other values of p are listed in Table 1(a). Figure 4(a) shows the shape of the intermediate point e_{M} on the initial path connecting u_1 and $-u_1$ we used for CMPA to find u_2 for all the listed values of p. The function u_2 found this way seems to posses an odd symmetry with respect to its nodal line. The slope of this nodal line in

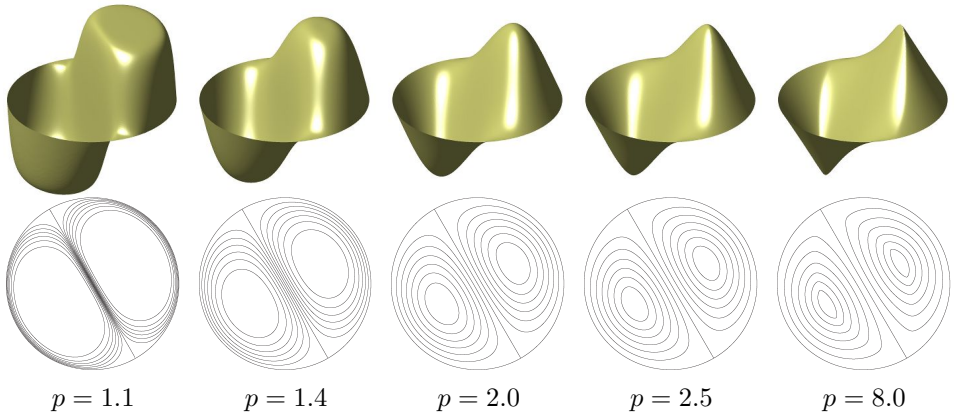

FIGURE 2. The numerically computed second eigenfunction u_2 for the disk.

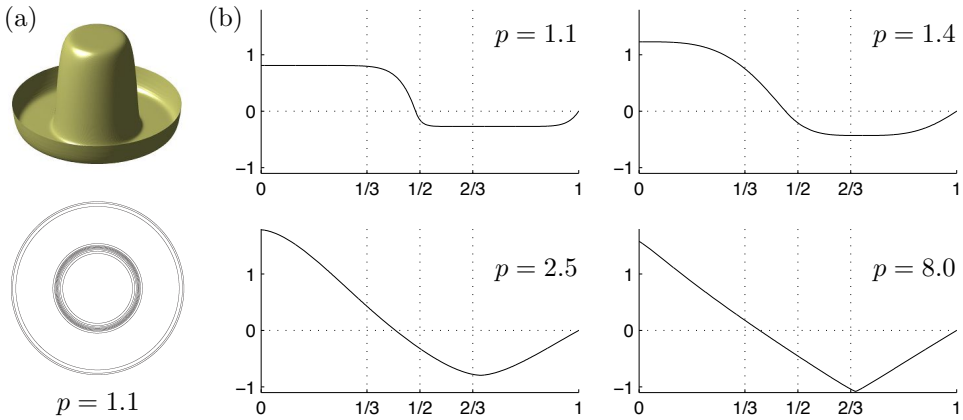

FIGURE 3. The numerically computed radially symmetric second eigenfunction u_2^{rad}: (a) using the genuine 2D method; (b) using the radial 2D method (the profile for the radial coordinate $r \in (0,1)$ is shown, scaled such that $\|u_2^{\mathrm{rad}}\|_p = 1$).

the coordinate system (x_1, x_2) depends on the computation. For the depiction in Fig. 2 we rotated Ω in each case to make the slope appear the same. CMPA needed between 120 and 600 iterations to converge.

Figure 4(b) shows an alternative shape of e_{M}. With such an initial path CMPA converged for $p = 1.1$ and $p = 1.2$ to a radially symmetric function we call u_2^{rad} (but for higher values of p to the oddly symmetric function u_2). Figure 3(a) shows u_2^{rad} for $p = 1.1$.

Figure 4(c) shows yet another choice of e_{M} (radially symmetric). With this intermediate point of the initial path and for $p = 1.3$ and $p = 1.4$ (but not larger) CMPA seems to converge to a radially symmetric function first but after many iterations the path slips down and the algorithm converges eventually to the oddly symmetric u_2. The graph in Fig. 4(d) shows how the maximum value of the Dirichlet

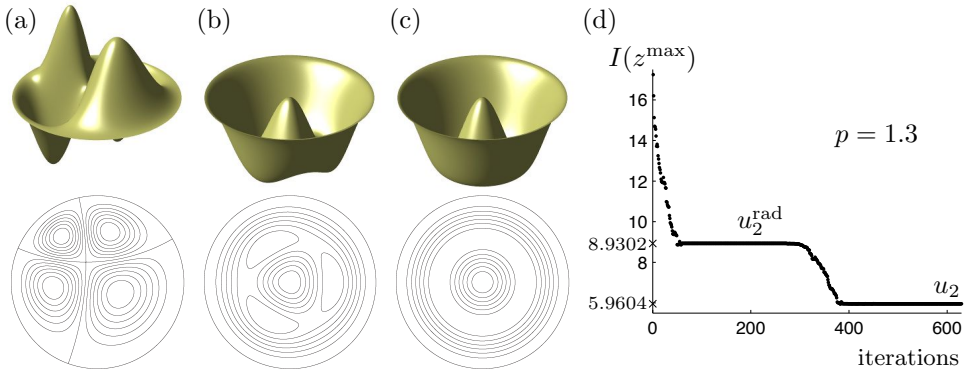

FIGURE 4. (a)–(c) Intermediate point $e_{\rm M}$ of the initial path used in CMPA. (d) Maximum value of the Dirichlet functional I along the path during the run of CMPA with $e_{\rm M}$ shown in (c) for $p = 1.3$.

functional I along the path develops during the run of the algorithm (for $p = 1.3$). The horizontal axis shows the number of iterations. The flat part between iterations 70 and 260 indicates that the path is staying close to a critical point. When now the norm of the descent direction $w_{z^{\max}}$ given in (3.9) computed at the "highest" point $z^{\max}$ of the path gets small enough, we stop the algorithm and save this highest point. Since it displays a radial symmetry, we call it $u_2^{\rm rad}$ again.

The eigenvalues $\lambda_2^{\rm rad}$ corresponding to the found $u_2^{\rm rad}$ are also listed in Table 1(a).

Figure 3(b) shows profiles of the eigenfunction $u_2^{\rm rad}$ computed by the radial 2D method for several values of p. The eigenvalues λ_1 and $\lambda_2^{\rm rad}$ computed by this method for these and other values of p are listed in Table 1(b). The convergence of CMPA does not seem to be sensitive to the choice of $e_{\rm M}$ in this case.

By comparing the values of λ_1 and $\lambda_2^{\rm rad}$ in Table 1(a) with those in Table 1(b) which were computed by the two different numerical methods we observe that their first three digits coincide in almost all the cases. Also, the profiles of u_1, $u_2^{\rm rad}$ are very close for both methods, respectively (cf. Fig 3(a) and the top left graph in (b) for $u_2^{\rm rad}$ and $p = 1.1$). We conclude that these are numerical approximations of the same eigenvalue-eigenfunction pairs.

The behavior of CMPA suggests that although $u_2^{\rm rad}$ is a constrained mountain pass point of I among radially symmetric functions, it is not a constrained mountain pass point with no assumption on the symmetry (cf. Fig. 4(d)). The cases of $p = 1.1$ and $p = 1.2$ when CMPA with $e_{\rm M}$ from Fig. 4(b) converged to a radially symmetric function and the path did not slip off to asymmetric functions with lower values of I seem to contradict this. However, we assume that this was caused by the "flat" shape of the landscape of I close to $u_2^{\rm rad}$ for p close to 1 and by numerical inaccuracies.

The dependence of λ_1, λ_2, and $\lambda_2^{\rm rad}$ on p is presented in Figs. 5 and 6. First of all we observe that for all the values of p considered the inequality $\lambda_2 < \lambda_2^{\rm rad}$ holds. Hence this is a numerical evidence that the second eigenfunction for the disk is not radially symmetric not only for small p but for a large range of p.

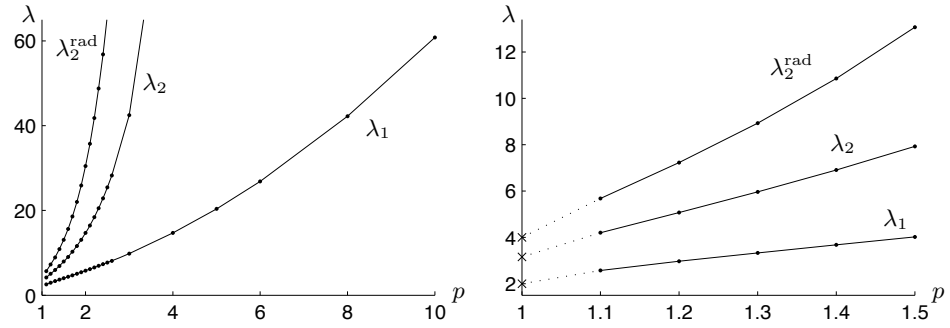

FIGURE 5. Dependence of the numerically computed eigenvalues for the disk on p. The three cross symbols in the graph on the right mark the values $h_1(\Omega) = 2$, $h_2(\Omega) \approx 3.1543$, and $h_2^{\rm rad}(\Omega) = 4$.

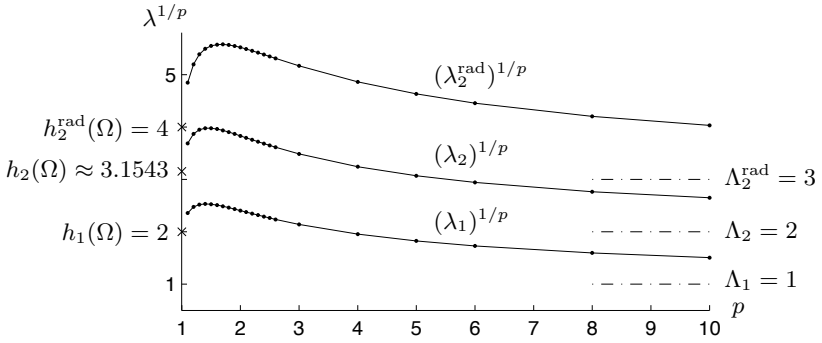

FIGURE 6. Dependence of the numerically computed eigenvalues for the disk raised to $1/p$ on p.

Second, we can observe the following asymptotic behavior:

	λ_1	λ_2	$\lambda_2^{\rm rad}$
$\lim_{p\to 1+} \lambda$	2	3.1543	4
$\lim_{p\to\infty} \lambda^{1/p}$	1	2	3

Theoretical results for λ_1 and λ_2 were summarized in Sec. 2. The values $h_1(\Omega)$, $\Lambda_1(\Omega)$, and $\Lambda_2(\Omega)$ for the disk are easy to compute. In [22] it was proved that $h_2(\Omega)$ for the disk equals the first Cheeger constant for the half-disk which is approximately 3.1543. We could observe that u_1 converges to 1 for $p \to 1$ as explained in [17] and to the distance function to the boundary for $p \to \infty$ as explained in [16]. In Fig. 2 we observe that for $p \to 1$ the function u_2 is getting close to the indicator function of the Cheeger set for the half-disk on each nodal domain.

In [5] a numerical evidence is given leading to the conjecture for the asymptotic behavior of $\lambda_2^{\rm rad}$ given in the above table. Our numerical results (at least for $p \to 1$) support this conjecture. To motivate these values and the profiles of $u_2^{\rm rad}$ in Fig. 3 we make the following two remarks:

Remark 4.1. 1. For $r \in (0,1)$ let $D(r)$ be the disk of radius r centered at the origin, $A(r) = \Omega \setminus \overline{D(r)}$ an annulus. It is easy to show that for $r = 1/2$ both D and A have the same Cheeger constant $h_2^{\mathrm{rad}}(\Omega) := h_1(D(1/2)) = h_1(A(1/2)) = 4$ (see, e.g., [19] for a result about the Cheeger constant of an annulus). The function u_2^{rad} with its profile shown in Fig. 3 seems to get close to the indicator function of $D(1/2)$ and $A(1/2)$ on each nodal domain for $p \to 1$.

2. Under the assumption of radial symmetry two largest disjoint disks of the same radius inscribed in Ω have radius 1/3. Hence we define $\Lambda_2^{\mathrm{rad}} = \frac{1}{1/3} = 3$. The function u_2^{rad} with its profile shown in Fig. 3 seems to get close on each nodal domain to a multiple of the function giving the distance to the boundary on $D(1/3)$ and $A(1/3)$ for large p.

4.2. **Square.** Let

$$\Omega := \left\{(x_1, x_2) \in \mathbb{R}^2 : x_1, x_2 \in (0,2)\right\}.$$

This domain was discretized using 83,968 triangles. Figure 7 shows the eigenfunction u_2 for several values of p. Table 2 lists the computed values of λ_1 and λ_2.

p	λ_1	λ_2	$\lambda_{\mathcal{S}_2}$
1.1	2.3649	3.7586	3.8702
1.2	2.6934	4.5012	4.6179
1.3	2.9986	5.2500	5.3715
1.4	3.2834	6.0385	6.1621
1.5	3.5611	6.8835	7.0053
1.6	3.8356	7.7971	7.9118
1.7	4.1092	8.7897	8.8903
1.8	4.3830	9.8708	9.9490
1.9	4.6581	11.050	11.095
2.0	4.9349	12.338	12.338

p	λ_1	λ_2	$\lambda_{\mathcal{S}_1}$
2.0	4.9349	12.338	12.338
2.1	5.2139	13.684	13.744
2.2	5.4952	15.144	15.282
2.3	5.7791	16.725	16.961
2.4	6.0658	18.438	18.797
2.5	6.3552	20.293	20.802
3.0	7.8452	32.107	33.956
4.0	11.038	74.757	85.447
5.0	14.497	163.59	205.08
6.0	18.194	343.77	477.60
8.0	26.221	1,402.1	2,443.4
10.0	34.990	5,339.0	11,888

TABLE 2. Eigenvalues for the square.

Various choices of the intermediate path point e_{M} were used to compute u_2. Only in case $p = 2$ different choices of e_{M} caused CMPA to converge to different functions u_2. Since for the square the eigenspace corresponding to the second eigenvalue of the Laplace operator is two-dimensional, CMPA converges to some member of this eigenspace depending on the shape of the initial path. Figure 7 shows one such eigenfunction. However, even for $p = 2$ this has no influence on the computed value of λ_2.

We say that a function has symmetry $\mathcal{S}_1$ (odd symmetry about $x_1 = 1$ and even symmetry about $x_2 = 1$) if it belongs to

$$\mathcal{S}_1 := \{u : \Omega \to \mathbb{R} : u(x_1, x_2) = -u(2 - x_1, x_2), u(x_1, x_2) = u(x_1, 2 - x_2)\},$$

and symmetry $\mathcal{S}_2$ (odd symmetry about $x_1 = x_2$ and even symmetry about $x_1 = 2 - x_2$) if it belongs to

$$\mathcal{S}_2 := \{u : \Omega \to \mathbb{R} : u(x_1, x_2) = -u(x_2, x_1), u(x_1, x_2) = u(2 - x_2, 2 - x_1)\}.$$

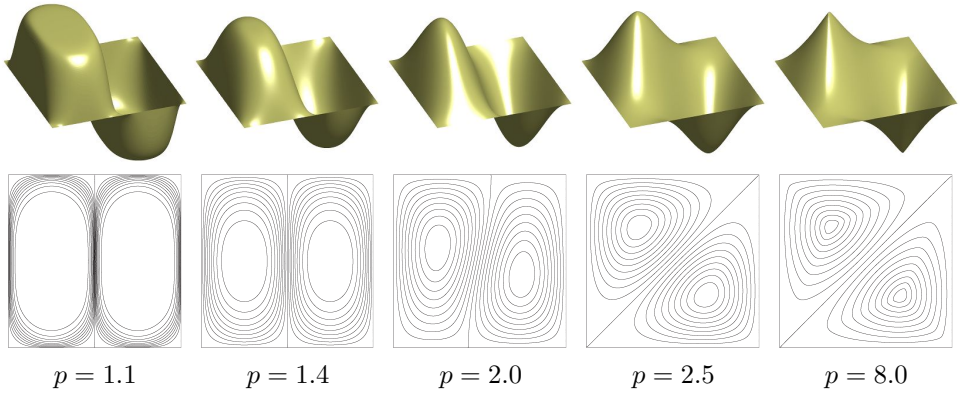

FIGURE 7. The numerically computed second eigenfunction u_2 for the square.

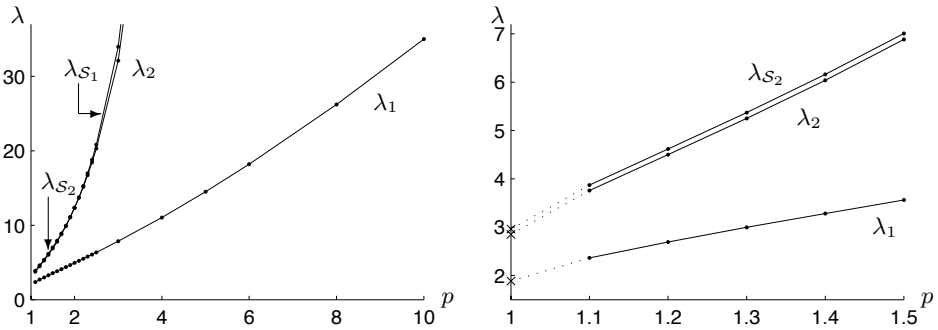

FIGURE 8. Dependence of the numerically computed eigenvalues for the square on p. The three cross symbols in the graph on the right mark the values of h_1 for Ω, Ω_1^{half}, and Ω_2^{half}.

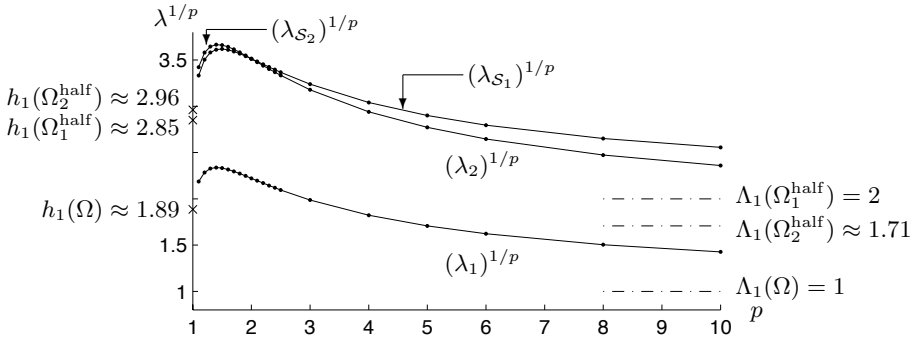

FIGURE 9. Dependence of the numerically computed eigenvalues for the square raised to $1/p$ on p.

(a)	$\lambda_{\mathcal{S}_1}$	$\lambda_{\mathcal{S}_2}$
$p < 2$	$= \lambda_2$	$> \lambda_2$
$2 < p$	$> \lambda_2$	$= \lambda_2$

(b)	λ_1	$\lambda_{\mathcal{S}_1}$	$\lambda_{\mathcal{S}_2}$
$\lim_{p\to 1+} \lambda$	$1 + \frac{1}{2}\sqrt{\pi}$	$\frac{4-\pi}{3-\sqrt{1+2\pi}}$	$1 + \frac{1}{2}(\sqrt{2} + \sqrt{2\pi})$
$\lim_{p\to\infty} \lambda^{1/p}$	1	2	$1 + \frac{1}{2}\sqrt{2}$

TABLE 3. The smallest eigenvalues $\lambda_{\mathcal{S}_1}$ and $\lambda_{\mathcal{S}_2}$ under symmetry assumptions for the square. (a) Numerical comparison with λ_2. (b) Asymptotic behavior: the first row shows values of h_1, the second row values of Λ_1 for Ω, Ω_1^{half}, and Ω_2^{half}, respectively.

As it was observed in [24], u_2 changes its symmetry at $p = 2$ from $\mathcal{S}_1$ for $p < 2$ to $\mathcal{S}_2$ for $p > 2$. Let $\lambda_{\mathcal{S}_i}$ denote the smallest eigenvalue with an eigenfunction belonging to $\mathcal{S}_i$ where $i \in \{1, 2\}$. The values of $\lambda_{\mathcal{S}_i}$ can be computed using CDM on Ω with additional boundary conditions $u(1, x_2) = 0$ for $x_2 \in (0, 2)$ or $u(x, x) = 0$ for $x \in (0, 2)$, respectively, or as the first eigenvalue on the half-domain Ω_i^{half}, where

$$\Omega_1^{\text{half}} := \{(x_1, x_2) \in \mathbb{R}^2 : x_1 \in (0, 1), x_2 \in (0, 2)\},$$
$$\Omega_2^{\text{half}} := \{(x_1, x_2) \in \mathbb{R}^2 : x_1 \in (0, 2), x_2 \in (0, x_1)\}.$$

Our numerical observations regarding these eigenvalues and λ_2 are summarized in Table 3(a) and the computed values are listed in Table 2. We stress that λ_2 was computed with no a priori assumptions on symmetry. The dependence of the eigenvalues λ_1, λ_2, $\lambda_{\mathcal{S}_1}$ and $\lambda_{\mathcal{S}_2}$ on p is further plotted in Figures 8 and 9.

These figures and Table 3(b) also explain the asymptotic behavior as $p \to 1$ and $p \to \infty$. While the table shows the limit values as given by the theory, the graphs indicate convergence to these values (at least for $p \to 1$; for $p \to \infty$ it seems a larger range of p would be needed). The Cheeger constants h_1 shown in the first row of Table 3(b) have been computed according to [17], [18] by

$$h_1\big((0, a) \times (0, b)\big) = \frac{4 - \pi}{a + b - \sqrt{(a - b)^2 + \pi ab}} \quad \text{for } a, b > 0. \tag{4.2}$$

The evaluation of Λ_1 in the second row is straightforward.

4.3. **Rectangle.** Let

$$\Omega := \big\{(x_1, x_2) \in \mathbb{R}^2 : x_1 \in (0, 2), x_2 \in (0, 1.75)\big\}.$$

This domain was discretized using 77,312 triangles. The shape of the first eigenfunction u_1 and the graph of the first eigenvalue $\lambda_1(\Omega; p)$ are similar to those for the square. However, the symmetry properties of the second eigenfunction u_2 are different: According to our numerical observations, for $p \le 3.6$ the eigenfunction u_2 preserves an odd symmetry about $x_1 = 1$ and an even symmetry about $x_2 = 0.875$ (which we call $\mathcal{S}_1$ as in the case of the square). For $p \ge 3.7$ this symmetry is lost and u_2 maintains an odd symmetry with respect to $(1, 0.875)$, the center of Ω. The contour lines of u_2 for several values of p are shown in Fig. 10.

For $p \ge 3.7$ the smallest eigenvalue $\lambda_{\mathcal{S}_1}$ corresponding to an eigenfunction with symmetry $\mathcal{S}_1$ is larger than λ_2 (cf. Fig. 11). This eigenpair can be computed by CDM on Ω with an additional boundary condition $u(1, x_2) = 0$ for $x_2 \in (0, 1.75)$ or as the first eigenpair on the half-rectangle

$$\Omega^{\text{half}} := \big\{(x_1, x_2) \in \mathbb{R}^2 : x_1 \in (0, 1), x_2 \in (0, 1.75)\big\}.$$

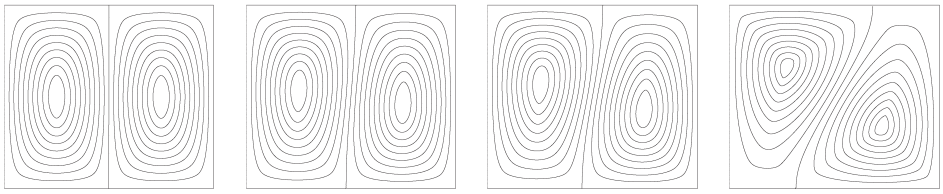

$p = 3.6$ $p = 3.7$ $p = 3.8$ $p = 8.0$

FIGURE 10. The numerically computed second eigenfunction u_2 for the rectangle.

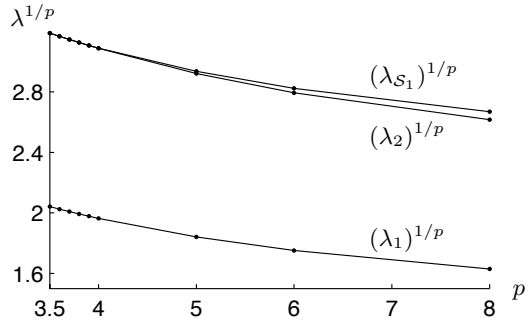

$\Omega = (0,2) \times (0,1.75)$

p	λ_1	λ_2	$\lambda_{\mathcal{S}_1}$
3.6	12.680	63.436	63.436
3.7	13.206	69.491	69.492
3.8	13.743	76.059	76.083
3.9	14.292	83.175	83.256
4.0	14.853	90.881	91.059
8.0	49.531	2,192.9	2,574.6

FIGURE 11. Comparison of the numerically computed second eigenvalue λ_2 and the smallest eigenvalue $\lambda_{\mathcal{S}_1}$ under the symmetry $\mathcal{S}_1$ for the rectangle Ω (λ_1 is shown for reference).

(a) Rectangle $(0,2) \times (0,1.9)$

p	λ_1	λ_2	$\lambda_{\mathcal{S}_1}$
2.44	6.5926	20.0177	20.0177
2.46	6.6579	20.4281	20.4281
2.48	6.7234	20.8451	20.8457
2.50	6.7891	21.2683	21.2708
2.60	7.1205	23.4816	23.5124

(b) Rectangle $(0,2) \times (0,1.6)$

p	λ_1	λ_2	$\lambda_{\mathcal{S}_1}$
5.6	36.077	383.4648	383.4648
5.8	38.898	453.2332	453.2333
6.0	41.892	535.2007	535.2009
6.2	45.068	631.4438	631.4478
6.4	48.437	744.1846	744.4026

TABLE 4. Comparison of the numerically computed second eigenvalue λ_2 and the smallest eigenvalue $\lambda_{\mathcal{S}_1}$ under the symmetry $\mathcal{S}_1$ for other rectangles.

Our conjecture is that for a rectangle $R = (0,a) \times (0,b)$ with $0 < b < a$ there exists $p_0 > 2$ such that u_2 has two nodal domains which for $p < p_0$ are rectangles with sides $a/2$ and b. For $p > p_0$ the nodal domains are not rectangular and u_2 has only an odd symmetry with respect to the center of R. According to our numerical observations, p_0 gets larger the larger the ratio a/b: Besides Ω we ran the computation for two other rectangles. For $R = (0,2) \times (0,1.9)$ the loss of symmetry $\mathcal{S}_1$ of u_2 is observable approximately between $p = 2.44$ and $p = 2.48$ and for $R = (0,2) \times (0,1.6)$ between $p = 5.6$ and $p = 6.0$ (cf. Table 4). As p grows

and crosses p_0, the nodal line which is straight for $p < p_0$ gets distorted. This distortion is faster for smaller ratios a/b (R closer to a square) and slower for larger ratios. For the square ($a = b$) it happens "immediately" at $p = 2$ since the passage from the the nodal line $x_1 = a/2$ to the nodal line $x_1 = x_2$ is realized within the two-dimensional eigenspace.

4.4. **Triangle with height 1.** Let

$$\Omega := \{(x_1, x_2) \in \mathbb{R}^2 : x_1 \in (0, 1), |x_2| < \frac{1}{2}(1 - x_1)\}$$

be an isosceles triangle with base 1 and height 1. It was discretized using 38,912 triangles. Figure 12 shows the eigenfunction u_2 for several values of p. Table 5 lists the computed values of λ_1 and λ_2.

p	λ_1	λ_2	p	λ_1	λ_2	$\lambda_{2,\mathcal{S}_E}$
1.1	8.0143	12.188	2.6	122.02	356.35	356.35
1.2	10.208	16.211	2.7	142.81	435.98	435.99
1.3	12.673	21.009	2.8	166.94	532.61	532.78
1.4	15.515	26.847	2.9	194.90	649.76	650.31
1.5	18.822	33.998	3.0	227.29	791.69	792.92
1.6	22.683	42.774	3.5	483.05	2,093.5	2,107.6
1.7	27.196	53.546	4.0	1,006.3	5,425.7	5,498.4
1.8	32.471	66.762	5.0	4,183.4	34,911	35,924
1.9	38.634	82.963	6.0	16,688	$2.1571 \cdot 10^5$	$2.2561 \cdot 10^5$
2.0	45.831	102.80	8.0	$2.4510 \cdot 10^5$	$7.6097 \cdot 10^6$	$8.2094 \cdot 10^6$
2.5	104.10	290.87	10.0	$3.3583 \cdot 10^6$	$2.5069 \cdot 10^8$	$2.7692 \cdot 10^8$

TABLE 5. Eigenvalues for the triangle with height 1.

Various intermediate path points e_M were used to compute u_2. However, the function that CMPA converged to did not depend on this choice. The symmetry properties of the computed u_2 depend only on the value p. For $p \le 2.6$ it is *even* in x_2, i.e., it belongs to

$$\mathcal{S}_E := \{u : \Omega \to \mathbb{R} : u(x_1, x_2) = u(x_1, -x_2)\}.$$

For $p \ge 2.7$ this symmetry is lost by u_2 as the graphs in Fig. 12 show.

For $p = 2.6$ the computation was repeated with intermediate path points e_M without symmetry $\mathcal{S}_E$ but CMPA always converged to the function shown in Fig. 12 which displays symmetry $\mathcal{S}_E$.

For $p = 2.7$ a symmetric $e_M \in \mathcal{S}_E$ was chosen. The graph in Fig. 13(a) shows how the maximum of the Dirichlet functional I along the path evolved during this run of CMPA. The path connecting u_1 with $-u_1$ which gets deformed at every step of CMPA seems to stay close to some critical point having symmetry $\mathcal{S}_E$ during the first 1,000 steps but then it slips down to lower values of I and stays close to another critical point. This is the asymmetric u_2 which the algorithm eventually converges to.

Even beyond $p = 2.6$ there exist eigenfunctions with symmetry $\mathcal{S}_E$. Let $u_{2,\mathcal{S}_E}$ denote a sign-changing eigenfunction of the p-Laplace operator on Ω which lies in

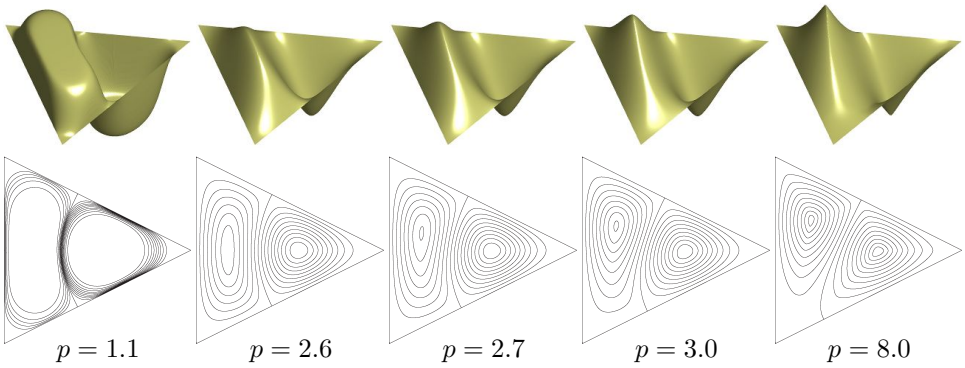

FIGURE 12. The numerically computed second eigenfunction u_2 for the triangle with height 1.

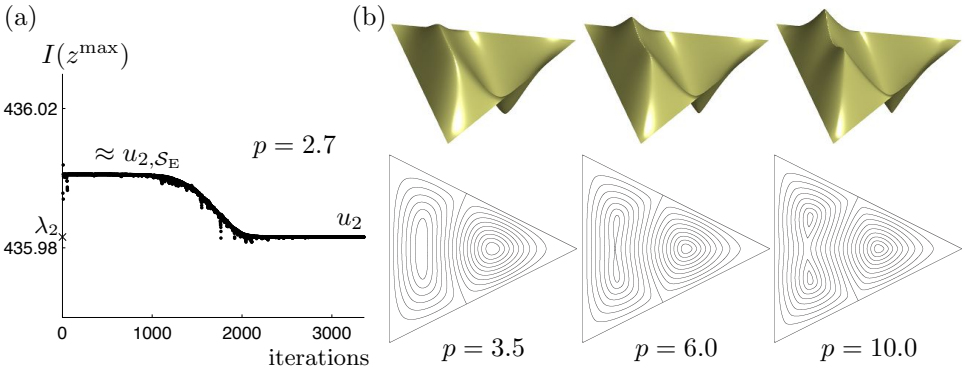

FIGURE 13. Triangle with height 1: (a) Maximum value of the Dirichlet functional I along the path during the run of CMPA for $p = 2.7$ and $e_M \in \mathcal{S}_E$. (b) The computed eigenfunction $u_{2,\mathcal{S}_E}$ for $p = 3.5, 6.0$, and 10.0.

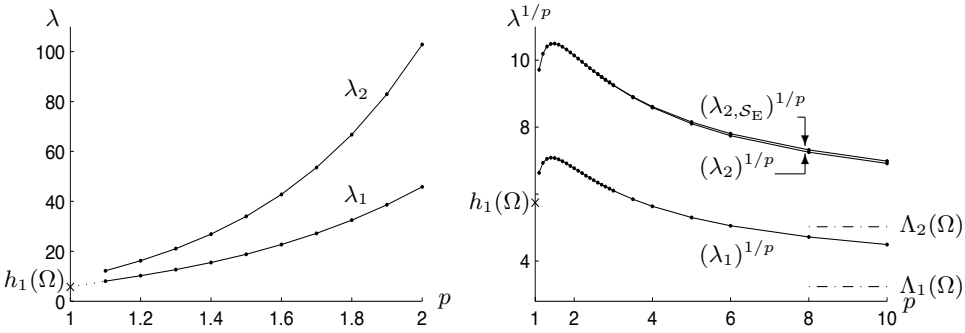

FIGURE 14. Dependence of the numerically computed eigenvalues for the triangle with height 1 on p.

$\mathcal{S}_{\mathrm{E}}$ and has the smallest eigenvalue (which we denote $\lambda_{2,\mathcal{S}_{\mathrm{E}}}$). As mentioned above, for $p \le 2.6$ we observed that $u_2 = u_{2,\mathcal{S}_{\mathrm{E}}}$ (up to scaling). To compute $u_{2,\mathcal{S}_{\mathrm{E}}}$ for $p \ge 2.7$ consider the eigenvalue problem

$$\begin{aligned} -\Delta_p u &= \lambda |u|^{p-2}u \quad \text{in } \Omega^{\mathrm{half}}, \\ \tfrac{\partial u}{\partial n} &= 0 \quad \text{on } \Gamma_1, \\ u &= 0 \quad \text{on } \Gamma_2, \end{aligned} \tag{4.3}$$

where

$$\begin{aligned} \Omega^{\mathrm{half}} &:= \{(x_1,x_2) \in \Omega : x_2 > 0\}, \\ \Gamma_1 &:= \big\{(x_1,x_2) \in \partial\Omega^{\mathrm{half}} : x_2 = 0\big\}, \\ \Gamma_2 &:= \partial\Omega^{\mathrm{half}} \setminus \Gamma_1. \end{aligned} \tag{4.4}$$

Any eigenfunction solving this problem can be extended to an eigenfunction on the whole Ω by even symmetry about $x_2 = 0$. Since the first eigenfunction of the original problem (1.1) for the triangle Ω belongs to $\mathcal{S}_{\mathrm{E}}$, its restriction to Ω^{half} is the first eigenfunction for (4.3). Hence to compute $u_{2,\mathcal{S}_{\mathrm{E}}}$ we just need to apply CMPA to problem (4.3) with paths which again connect u_1 and $-u_1$. The modification of the finite element method to take into account the natural boundary condition on Γ_1 is straightforward. The computed values of $\lambda_{2,\mathcal{S}_{\mathrm{E}}}$ are listed in Table 5. Figure 13(b) shows the corresponding eigenfunction $u_{2,\mathcal{S}_{\mathrm{E}}}$ for selected values of p.

The dependence of the eigenvalues λ_1, λ_2, and $\lambda_{2,\mathcal{S}_{\mathrm{E}}}$ on p is further plotted in Fig. 14. The figure also shows the limits of λ_1 for $p \to 1$ and ∞ and of λ_2 for $p \to \infty$ which can be computed explicitly. As mentioned, for example, in [18], the Cheeger constant of a triangle is given by $h_1(\Omega) = (\mathrm{Per}(\Omega) + \sqrt{4\pi|\Omega|})/(2|\Omega|)$ and hence in our case $h_1(\Omega) = 1 + \sqrt{5} + \sqrt{2\pi} \approx 5.7427$. Simple computations yield $\Lambda_1(\Omega) = 1 + \sqrt{5} \approx 3.2361$ and $\Lambda_2(\Omega) = 1 + 9/\sqrt{5} \approx 5.0249$.

4.5. **Triangle with height 3/4.** Let

$$\Omega := \big\{(x_1,x_2) \in \mathbb{R}^2 : x_1 \in \big(0, \tfrac{3}{4}\big), |x_2| < \tfrac{2}{3}\big(\tfrac{3}{4} - x_1\big)\big\}$$

be an isosceles triangle with base 1 and height 3/4. It was discretized using 28,672 triangles. Figure 15 shows the eigenfunction u_2 for several values of p. Table 6 lists the computed values of λ_1 and λ_2.

p	λ_1	λ_2	$\lambda_{\mathcal{S}_{\mathrm{O}}}$	p	λ_1	λ_2	p	λ_1	λ_2
1.1	9.389	14.38	14.50	1.8	42.07	86.84	2.5	149.1	413.0
1.2	12.13	19.41	19.52	1.9	50.78	109.2	3.0	350.0	1,196
1.3	15.28	25.53	25.62	2.0	61.11	137.1	4.0	1,789	9,351
1.4	18.97	33.10	33.17	2.1	73.36	171.6	5.0	8,591	$6.87 \cdot 10^4$
1.5	23.35	42.52	42.55	2.2	87.85	214.4	6.0	$3.95 \cdot 10^4$	$4.84 \cdot 10^5$
1.6	28.55	54.22	54.22	2.3	105.0	267.2	8.0	$7.75 \cdot 10^5$	$2.23 \cdot 10^7$
1.7	34.73	68.76	68.76	2.4	125.2	332.5	10.0	$1.41 \cdot 10^7$	$9.60 \cdot 10^8$

TABLE 6. Eigenvalues for the triangle with height 3/4.

The symmetry properties of the computed u_2 change again with p. For this triangle, however, u_2 gains more symmetry as p increases (unlike for the triangle

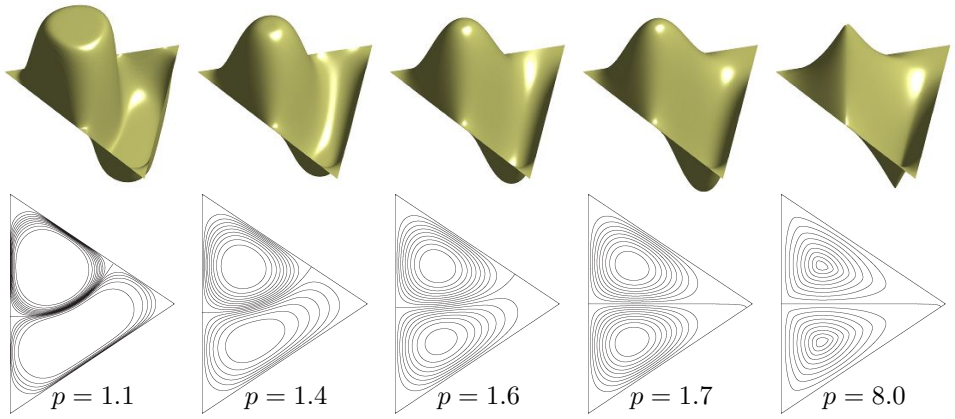

FIGURE 15. The numerically computed second eigenfunction u_2 for the triangle with height 3/4.

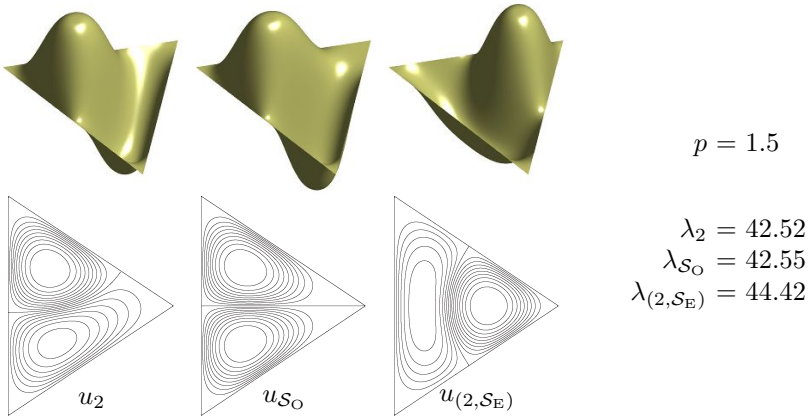

FIGURE 16. Higher eigenfunctions for the triangle with height 3/4 for $p = 1.5$: u_2 and $u_{(2,\mathcal{S}_E)}$ computed as constrained local mountain pass points by CMPA with no a priori assumptions on symmetry, $u_{\mathcal{S}_O}$ computed by CDM enforcing symmetry $\mathcal{S}_O$.

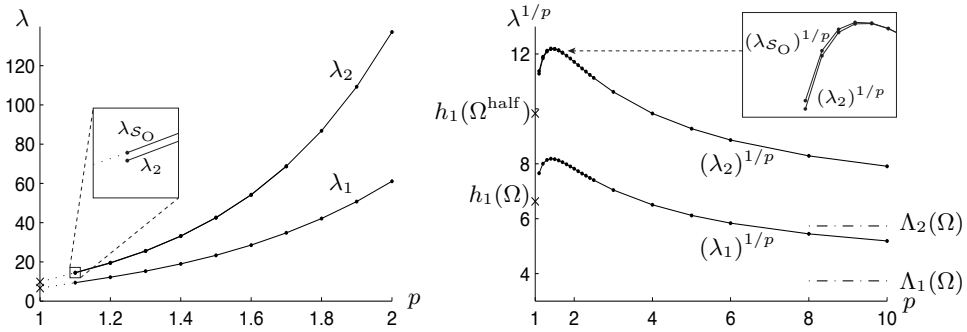

FIGURE 17. Dependence of the numerically computed eigenvalues for the triangle with height 3/4 on p.

with height 1 where u_2 lost symmetry). For $p \le 1.6$ the nodal line of u_2 connects the base of the triangle with one of its other sides. For $p \ge 1.7$ this nodal line connects the base with the vertex above the base and u_2 is *odd* in x_2, i.e., it belongs to

$$\mathcal{S}_{\mathrm{O}} := \{u : \Omega \to \mathbb{R} : u(x_1, x_2) = -u(x_1, -x_2)\}$$

as can be seen in Fig. 15. It is because of lack of resolution of the numerical method close to the vertex (where u_2 is flat) that the zero contour line in the figure for $p = 1.7$ and $p = 8.0$ does not exactly reach the vertex.

For $p \le 1.6$ there also exist eigenfunctions with symmetry $\mathcal{S}_{\mathrm{O}}$. Let $\lambda_{\mathcal{S}_{\mathrm{O}}}$ denote the smallest eigenvalue with an eigenfunction belonging to $\mathcal{S}_{\mathrm{O}}$ (denoted $u_{\mathcal{S}_{\mathrm{O}}}$). Using the notation defined in (4.4) this eigenvalue can be computed using CDM on Ω with an additional boundary condition $u = 0$ on Γ_1 or as the first eigenvalue on the half-domain Ω^{half}. The computed values of $\lambda_{\mathcal{S}_{\mathrm{O}}}$ are also listed in Table 6. For $p \ge 1.7$ the values of λ_2 and $\lambda_{\mathcal{S}_{\mathrm{O}}}$ coincide. For $p = 1.6$ they differ in the sixth digit.

As in the previous computations, various choices of the intermediate path point e_{M} were used to compute u_2 on Ω with no a priori assumptions on symmetry. In some cases CMPA converged to different functions depending on this choice (different local mountain passes). For example, for $p = 1.5$ two eigenfunctions were found: one with a nodal line connecting the base of the triangle with one of its sides, and another one with a nodal line connecting the two sides and having an even symmetry in x_2. Both eigenfunctions are (numerically) local mountain pass points of I with respect to the constraint S. The first one is called u_2 since it has the smallest eigenvalue, the second one is called $u_{(2,\mathcal{S}_{\mathrm{E}})}$ because of its symmetry (it could also be understood as a solution of (4.3) formulated in a similar way for the triangle with height 3/4). Both eigenfunctions are shown in Fig. 16 together with $u_{\mathcal{S}_{\mathrm{O}}}$ for comparison.

The dependence of the eigenvalues λ_1, λ_2, and $\lambda_{\mathcal{S}_{\mathrm{O}}}$ on p is further plotted in Fig. 17. The following limits of λ_1 and $\lambda_{\mathcal{S}_{\mathrm{O}}}$ as $p \to 1$ and those of λ_1 and λ_2 as $p \to \infty$ are also marked in the figure and have these respective values:

$$h_1(\Omega) = \tfrac{2}{3}(2 + \sqrt{13} + \sqrt{6\pi}) \approx 6.631, \quad \Lambda_1(\Omega) = \tfrac{2}{3}(2 + \sqrt{13}) \approx 3.737,$$
$$h_1(\Omega^{\mathrm{half}}) = \tfrac{2}{3}(5 + \sqrt{13} + 2\sqrt{3\pi}) \approx 9.830, \quad \Lambda_2(\Omega) = \tfrac{2}{3}(5 + \sqrt{13}) \approx 5.737.$$

4.6. **Equilateral triangle.** For isosceles triangles close but not equal to an equilateral triangle a similar observation has been made as for rectangles close but not equal to the square: the symmetry properties of the second eigenfunction u_2 change at a certain value $p \ne 2$. According to the following computations, for an equilateral triangle this change occurs at $p = 2$ (as it does for the square).

Let

$$\Omega := \{(x_1, x_2) \in \mathbb{R}^2 : x_1 \in \Big(0, \frac{\sqrt{3}}{2}\Big), |x_2| < \frac{1}{\sqrt{3}}\Big(\frac{\sqrt{3}}{2} - x_1\Big)\}$$

be an equilateral triangle with side 1. It was discretized using 32,256 triangles. With the notation introduced in (4.4) we can define $\lambda_{2,\mathcal{S}_{\mathrm{E}}}$ and $u_{2,\mathcal{S}_{\mathrm{E}}}$ as in Sec. 4.4 and $\lambda_{\mathcal{S}_{\mathrm{O}}}$ and $u_{\mathcal{S}_{\mathrm{O}}}$ as in Sec. 4.5.

Our numerical observations are summarized in Table 7 and Fig. 18: For $p < 2$ the second eigenfunction u_2 is even in x_2 while for $p > 2$ it is odd (up to a rotation of the triangle by $\pm 2\pi/3$). We note that the values λ_2 listed in the table were computed with no a priori assumptions on the symmetry of u and then compared to the computed values $\lambda_{2,\mathcal{S}_{\mathrm{E}}}$ and $\lambda_{\mathcal{S}_{\mathrm{O}}}$. The corresponding eigenfunctions u_2 are

p	λ_1	$\lambda_2(=\lambda_{2,\mathcal{S}_\mathrm{E}})$	$\lambda_{\mathcal{S}_\mathrm{O}}$
1.1	8.653	13.37	13.61
1.9	44.07	98.20	98.40
2.0	52.64	122.8	122.8

p	λ_1	$\lambda_2(=\lambda_{\mathcal{S}_\mathrm{O}})$	$\lambda_{2,\mathcal{S}_\mathrm{E}}$
2.0	52.64	122.8	122.8
2.1	62.71	152.9	153.2
8.0	$4.240 \cdot 10^5$	$1.483 \cdot 10^7$	$1.668 \cdot 10^7$

TABLE 7. Eigenvalues for the equilateral triangle with side 1.

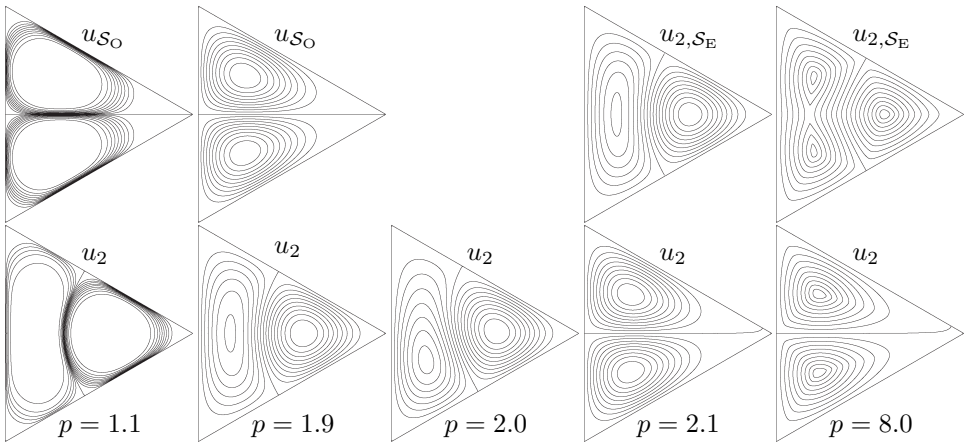

FIGURE 18. The numerically computed eigenfunctions u_2, $u_{2,\mathcal{S}_\mathrm{E}}$ and $u_{\mathcal{S}_\mathrm{O}}$ for the equilateral triangle.

in the bottom row of the figure. For $p = 2$ the eigenspace belonging to λ_2 is two-dimensional. The member of this eigenspace u_2 to which CMPA converges depends on the initial path, i.e., on the choice of the intermediate point e_M. The figure shows one such member. As already mentioned in Sec. 4.5, it is an artifact of the numerical method that for u_2 and $p = 2.1, 8.0$ the zero contour line does not exactly reach the vertex, where u_2 is rather flat.

5. Remarks on the numerics

5.1. **Dependence on the mesh parameter h.** Let $\mathcal{T}^h$ denote the set of all the triangles of a triangulation of Ω^h. The mesh parameter h was introduced in Sec. 3.1 as the (smallest) upper bound on the diameter of the circumscribed circle for triangles of $\mathcal{T}^h$. In this section the dependence of the computed values of λ_1 and λ_2 on h is investigated. The investigation is conducted for one particular domain Ω—the rectangular domain used for computations in Sec. 4.3:

$$\Omega := \{(x_1, x_2) \in \mathbb{R}^2 : x_1 \in (0, 2), x_2 \in (0, 1.75)\}.$$

Four discretizations of this domain are used. Table 8 lists details about these discretizations ordered by the number of triangles. Essentially, a finer mesh was obtained from a courser one by placing a new vertex in the middle of each triangle side of the old triangulation, in effect dividing each triangle in four.

Table 9 shows the values of λ_1 and λ_2 computed for the four triangulations characterized by h and for selected values of p. Figure 19 gives perhaps a more telling

$\mathcal{T}^h$	h	number of triangles
course	0.079	4,832
	0.044	19,328
	0.022	77,312
fine	0.011	309,248

TABLE 8. Triangulations used to discretize the rectangular domain Ω.

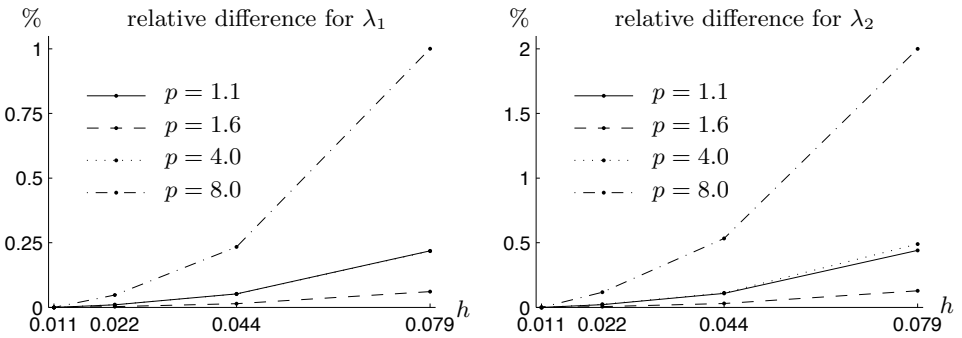

FIGURE 19. Relative difference $\frac{\lambda(\mathcal{T}^h)-\lambda(\mathcal{T}^{.011})}{\lambda(\mathcal{T}^{.011})} \cdot 100\%$ for λ_1 (left) and λ_2 (right) computed on a triangulation $\mathcal{T}^h$ with respect to the finest triangulation $\mathcal{T}^{.011}$. For λ_1 the relative differences for $p = 1.1$ and $p = 4.0$ almost coincide and cannot be distinguished in the graph.

	$p = 1.1$		$p = 1.6$		$p = 4.0$		$p = 8.0$	
h	λ_1	λ_2	λ_1	λ_2	λ_1	λ_2	λ_1	λ_2
0.079	2.5586	3.9507	4.2965	8.2462	14.884	91.306	50.005	2,234.8
0.044	2.5544	3.9376	4.2945	8.2381	14.859	90.962	49.625	2,202.7
0.022	2.5533	3.9342	4.2940	8.2361	14.853	90.881	49.533	2,193.6
0.011	2.5531	3.9334	4.2939	8.2356	14.851	90.861	49.510	2,191.0

TABLE 9. Values of λ_1 and λ_2 computed for four different triangulations of the rectangular domain Ω and $p = 1.1, 1.6, 4.0, 8.0$.

picture: for each p it displays relative differences $(\lambda(\mathcal{T}^h)-\lambda(\mathcal{T}^{.011}))/\lambda(\mathcal{T}^{.011})$, where $\lambda(\mathcal{T}^h)$ denotes the eigenvalue computed on the triangulation $\mathcal{T}^h$. The finest triangulation $\mathcal{T}^{.011}$ is used as a reference. We observe that the largest differences occur for large p (here $p = 8.0$) and smallest differences for p close to 2. The differences are about twice as large for λ_2 computed by CMPA compared to λ_1 computed by CDM.

5.2. **The Augmented Lagrangian Method.** As described in Sec. 3.3 this method is used to solve (3.10) iteratively for a given right-hand side. The Augmented Lagrangian $\mathcal{L}_r$ defined in (3.12) depends on a parameter $r > 0$. As observed by the authors of [13] the algorithm is not very sensitive to the choice of r but the analysis of the influence of r on the behavior of the algorithm is complicated.

The choice of r has an influence on the speed of convergence of the algorithm and at the same time on how precise the found numerical solutions can be. In general, for larger r the algorithm seems to converge faster but it is able to find only less precise approximations of the solution. For our computations we tried various values of r first and then chose the one which seemed to give a reasonable speed of convergence together with acceptable residual. This value depended strongly on p and also on the particular domain Ω. Table 10 shows the dependence of r and of the number of iterations that the algorithm needed on p. For each domain one value of r was chosen from the given range. Similarly, the number of iterations lay in the given range. We can observe that for a small p a large r was needed, for a large p a smaller r. For p close to 2 we could choose $r \approx 1$. The number of iterations needed turned larger for p farther from 2.

p	range of r	# of iterations
1.1	10^4 – 10^7	700 – 2,000
1.2	500 – 2,500	500 – 1,000
1.8	1 – 1.5	80 – 90
3.0	0.3 – 0.4	200 – 300
10.0	0.03 – 0.1	1,200 – 3,000

TABLE 10. The dependence of the approximate values of r and numbers of iterations in the Augmented Lagrangian Method on p.

We note that for values of p smaller than 1.1 and larger than 10 (the particular value also depended on the domain) we were not able to find r giving satisfactory results for our implementation of the Augmented Lagrangian Method in conjunction with CMPA.

5.3. **CDM and CMPA.** In both the Constrained Descent Method and the Constrained Mountain Pass Algorithm the measure of convergence is $\|w_u\|$, the $W_0^{1,p}(\Omega)$-norm of the descent direction evaluated at the approximation u of the eigenfunction which is being computed. The smallest achieved value depended on the algorithm, on p, and in case of CMPA also on the fact whether there lies another critical point not far from u. For CDM the order of this value was between 10^{-5} and 10^{-8}, for CMPA between 10^{-3} and 10^{-7}. The number of iterations of CDM was approximately between 10 and 30. The number of iterations of CMPA varied, it depended on the shape of the initial path and on p, and was anywhere between 100 and 3,000.

6. Conclusion

In this work a concrete application of the variational numerical methods of [14] in a Banach space was presented. In particular, one possible choice of the descent

direction required by these methods was proposed, implemented and tried in computations in the setting of the Sobolev space $W_0^{1,p}(\Omega)$. The computations yielded approximations of the smallest two Dirichlet eigenvalues and the corresponding eigenfunctions of the p-Laplace operator on several planar domains for p ranging from 1.1 to 10. This relatively large range made it possible to study the change of symmetry of the second eigenfunction with varying p on different domains which was first observed in [24] for the square and p not far from 2. The computed eigenvalues seem to agree with the asymptotic behavior known from theory for $p \to 1$. Our range of p seems to be too small, however, in order to clearly observe the asymptotic behavior of the eigenpairs as $p \to \infty$.

Numerical experiments were conducted for the following domains: the disk, rectangles, and isosceles triangles. We summarize the main observations about the symmetry of the second eigenfunction u_2. For the disk it was observed that u_2 has a straight nodal line dividing the disk into halves for the whole range of p.

For rectangles which are not a square and for small p the second eigenfunction is odd about its nodal line which is straight and connects the midpoints of the longer sides. After p crosses some value $p_0 > 2$ there are two second eigenfunctions which are mirror images of each other. Their nodal line is not straight but still connects the two longer sides.

For the square and $p \neq 2$ there are two second eigenfunctions which are images of each other under rotations by $\pi/2$ about the center of the square. For $p < 2$ their nodal line is straight and connects the midpoints of the opposite sides. For $p > 2$ the nodal line is a diagonal of the square. For $p = 2$ there are two linearly independent second eigenfunctions.

The symmetry observations for triangles are based on the family of isosceles triangles with vertices $(0, -1/2)$, $(0, 1/2)$, and $(\ell, 0)$ with base 1 and height $\ell > 0$ which are symmetric about the x_1-axis. For those shorter than the equilateral triangle and for small p there are two asymmetric second eigenfunctions (up to scaling) which are symmetry images of each other. Their nodal line connects the base with one side of the triangle. After p crosses some value $p_0 < 2$ there is only one eigenfunction u_2. It is odd about its nodal line which is straight and connects the middle of the base with the opposite vertex (symmetry $\mathcal{S}_{\mathrm{O}}$).

For triangles longer than the equilateral triangle and for small p there is one eigenfunction u_2, it is even about the x_1-axis (symmetry $\mathcal{S}_{\mathrm{E}}$) and its nodal line connects the two sides of the triangle. After p crosses some value $p_0 > 2$ there are two asymmetric second eigenfunctions which are symmetry images of each other. Their nodal line still connects the two sides of the triangle.

For the equilateral triangle and $p \neq 2$ there are three second eigenfunctions which are images of each other under rotations of the triangle about its midpoint by $\pm 2\pi/3$. For $p < 2$ their nodal line connects two sides of the triangle and they have even symmetry about the height coming from the third side. For $p > 2$ the nodal line of the second eigenfunctions follows a height of the triangle and the eigenfunctions have odd symmetry about this height. For $p = 2$ there are two linearly independent second eigenfunctions.

Figure 16 indicates that our numerical methods could be used for finding some higher eigenfunctions and perhaps for a continuation in ℓ to observe the connection between these eigenfunctions and the second eigenfunctions for the equilateral triangle. This lies however beyond the scope of this paper.

7. Appendix

Here we give a proof of some claims used in Sections 3.2 and 3.4. A subindex notation will be used for general sequences and does not refer to the enumeration of eigenfunctions and eigenvalues in this section.

Lemma 7.1. *Let I and J be defined by (2.1) and S by (2.3). Further, let $u \in S$ and*

$$w_u := -u + \frac{1}{\int_\Omega |u|^{p-2}u\, v_u\, dx}\, v_u, \quad \text{where } v_u := (-\Delta_p)^{-1}\left(|u|^{p-2}u\right). \tag{7.1}$$

Then $\langle I'(u), w_u\rangle \le 0$. Equality holds if and only if u is a critical point of I with respect to S which is the case if and only if $w_u = 0$.

The proof of this lemma is based on the following inequality which is a direct consequence of the Cauchy-Schwarz and Hölder inequalities. Its proof is therefore omitted.

Lemma 7.2. *Let $f, g \in W_0^{1,p}(\Omega)$, $f \neq 0$. Then*

$$\int_\Omega |\nabla f|^{p-2}\nabla f \nabla g\, dx \le \|f\|^{p-1}\|g\|.$$

Equality holds if and only if there exists $\nu \ge 0$ such that $\nu f = g$.

Proof of Lemma 7.1. We observe that

$$\int_\Omega |u|^{p-2}u\, v_u\, dx = \int_\Omega (-\Delta_p v_u) v_u\, dx = \|v_u\|^p. \tag{7.2}$$

By the definition of w_u, (7.2) and the auxiliary lemma we obtain

$$\begin{aligned}\langle I'(u), w_u\rangle &= -\|u\|^p + \frac{1}{\|v_u\|^p}\int_\Omega |\nabla u|^{p-2}\nabla u \nabla v_u\, dx \\ &\overset{(*)}{\le} -\|u\|^p + \frac{1}{\|v_u\|^p}\|u\|^{p-1}\|v_u\| = \Big(-1 + \frac{1}{\|v_u\|^{p-1}\|u\|}\Big)\|u\|^p.\end{aligned} \tag{7.3}$$

Using $u \in S$, testing the equation $-\Delta_p v_u = |u|^{p-2}u$ by u, and applying Lemma 7.2 yields

$$1 = \int_\Omega |u|^p\, dx = \int_\Omega |\nabla v_u|^{p-2}\nabla v_u \nabla u\, dx \overset{(**)}{\le} \|v_u\|^{p-1}\|u\|. \tag{7.4}$$

By combining (7.3) and (7.4) we conclude that $\langle I'(u), w_u\rangle \le 0$. Equality holds if and only if equality holds in $(*)$ and $(**)$. According to the auxiliary lemma this is the case if and only if $\nu u = v_u$ for some $\nu > 0$. Finally, we argue that the following are equivalent:

(a) $\nu u = v_u$ for some $\nu > 0$,
(b) u is a critical point of I with respect to S,
(c) $w_u = 0$.

Statement (a) is equivalent to $\nu^{p-1}(-\Delta_p u) = |u|^{p-2}u$ and hence to (b). If (a) holds, then $\int_\Omega |u|^{p-2}u\, v_u\, dx = \nu$ because $u \in S$. Hence $w_u = -u + \frac{1}{\nu}v_u = 0$ and (c) holds, too. It is obvious that (c) implies (a). □

Before stating the next proposition we recall some known results (let $p, q \in (1,\infty)$, $\frac{1}{p} + \frac{1}{q} = 1$):

(i) The p-Laplace operator $-\Delta_p : W_0^{1,p}(\Omega) \to W^{-1,q}(\Omega)$ is uniformly continuous on bounded sets.
(ii) The mapping $u \mapsto |u|^{p-2}u : W_0^{1,p}(\Omega) \to W^{-1,q}(\Omega)$ is compact and uniformly continuous on bounded sets.
(iii) The inverse p-Laplace operator $(-\Delta_p)^{-1} : W^{-1,q}(\Omega) \to W_0^{1,p}(\Omega)$ is uniformly continuous on bounded sets.

Both claims (i) and (ii) follow from standard inequalities found, e.g., in [13, Lemmas 5.3 and 5.4]. The compactness in (ii) follows from the compact embedding of $W_0^{1,p}(\Omega)$ in $L^p(\Omega)$. Claim (iii) follows from standard inequalities found, i.e., in [13, Propositions 5.1 and 5.2].

Proposition 7.3. *Let I and J be defined by* (2.1) *and S by* (2.3). *The initial value problem*

$$\frac{d}{dt}u(t) = w_{u(t)}, \quad u(0) = e_0 \in S \tag{7.5}$$

with w_u defined in (7.1) *has a unique solution $u(t) \in S$ defined for $t \in (0,\infty)$. There exists a critical point $u \in S$ of I with respect to S and a sequence $\{t_n\}_{n=1}^{\infty}$ such that $\lim_{n\to\infty} t_n = \infty$ and $\lim_{n\to\infty} u(t_n) = u$ in $W_0^{1,p}(\Omega)$.*

Proof. The proof of existence of a solution and its uniqueness follows the same lines as the proof of Lemma 5 in [14]. Hence we focus on establishing the existence of the sequence $\{t_n\}$.

Since $0 \le I(u(T)) = I(e_0) + \int_0^T \langle I'(u(t)), w_{u(t)}\rangle dt$ for $T > 0$ and the integrand is non-positive, we obtain $\int_0^\infty \left|\langle I'(u(t)), w_{u(t)}\rangle\right| dt \le I(e_0)$. Hence there exists a sequence $\{t_n\}_{n=1}^{\infty}$ with $\lim_{n\to\infty} t_n = \infty$ such that for $u_n := u(t_n)$ and $w_n := w_{u(t_n)}$ it holds:

$$\langle I'(u_n), w_n\rangle \to 0 \quad \text{for } n \to \infty. \tag{7.6}$$

We recall that by (7.1) and (7.2) we have

$$w_n = -u_n + \frac{1}{\|v_n\|^p} v_n, \quad \text{where } v_n := (-\Delta_p)^{-1}\left(|u_n|^{p-2}u_n\right). \tag{7.7}$$

We observe that $\{u_n\}$ is a bounded sequence, hence it converges weakly to some $u \in W_0^{1,p}(\Omega)$ along a subsequence which we again denote $\{u_n\}$. From the compactness of the map $u \mapsto |u|^{p-2}u$ and the continuity of the inverse p-Laplacian it follows that

$$v_n \to v := (-\Delta_p)^{-1}\left(|u|^{p-2}u\right) \quad \text{strongly in } W_0^{1,p}(\Omega) \text{ as } n \to \infty. \tag{7.8}$$

Equation (7.7) and the fact that $w_n \in T_{u_n}S$ imply

$$\langle -\Delta_p(w_n + u_n), w_n\rangle = \frac{1}{\|v_n\|^{p(p-1)}} \int_\Omega |u_n|^{p-2}u_n w_n \, dx = 0. \tag{7.9}$$

Combining (7.6) and (7.9) yields

$$\int_\Omega \left(|\nabla(w_n + u_n)|^{p-2}\nabla(w_n + u_n) - |\nabla u_n|^{p-2}\nabla u_n\right)\nabla w_n \, dx \to 0 \quad \text{for } n \to \infty. \tag{7.10}$$

On the other hand standard estimates [13, Propositions 5.1 and 5.2] state that

$$\begin{aligned}
&\int_\Omega \big(|\nabla(w_n+u_n)|^{p-2}\nabla(w_n+u_n) - |\nabla u_n|^{p-2}\nabla u_n\big)\nabla w_n\,dx \\
&\geq \delta\,\frac{\|w_n\|^2}{(\|w_n+u_n\|+\|u_n\|)^{2-p}} \quad \text{for } 1<p\leq 2, \\
&\geq \frac{1}{2^{p-2}}\|w_n\|^p \quad \text{for } 2\leq p,
\end{aligned}$$

where $\delta>0$ is a constant which does not depend on w_n and u_n. These inequalities and (7.10) imply

$$w_n \to 0 \quad \text{strongly in } W_0^{1,p}(\Omega) \text{ as } n\to\infty. \tag{7.11}$$

This and (7.7) in turn imply that $\{u_n\}$ converges strongly to u and that

$$u = \frac{1}{\|v\|^p}(-\Delta_p)^{-1}\left(|u|^{p-2}u\right), \tag{7.12}$$

which means that u is a critical point of I with respect to S. □

Remark 7.4. To better understand the implications of the choice of the descent direction we remark how the proof of the proposition would change if we used the steepest descent direction instead of the descent direction given by (7.1). Up to normalization the steepest descent direction w defined by (3.5) can be written as the solution of

$$-\Delta_p w = \Delta_p u + \alpha|u|^{p-2}u$$

for a suitable α. Testing this equation by w and using $w\in T_uS$ yields $\|w\|^p = -\frac{1}{p}\langle I'(u),w\rangle$. Hence equation (7.6) would directly imply $w_n\to 0$. We can write

$$0 \leftarrow \|w_n\|^{p-1} = \|-\Delta_p w_n\|_* = \left\|-\Delta_p u_n - \alpha_n|u_n|^{p-2}u_n\right\|_* = \frac{1}{p}\left\|I'(u_n)-\alpha_n J'(u_n)\right\|_*,$$

where $\|\cdot\|_*$ denotes the norm in the dual space $W^{-1,q}(\Omega)$. If we define $\|I'|_{S_u}\| := \inf_{\alpha\in\mathbb{R}}\|I'(u)-\alpha J'(u)\|_*$ as in [6], [14], then we would obtain $\|I'|_{S_{u_n}}\|\to 0$. The Palais-Smale condition under constraints which was formulated in [6] states in its simplified form that if $\{I'(u_n)\}$ is bounded and $\|I'|_{S_{u_n}}\|\to 0$ then $\{u_n\}$ possesses a convergent subsequence. In [9] it was shown that this condition holds in our setting. Hence the choice of the steepest descent direction would yield a more "classical" proof of the proposition.

References

[1] A. Anane, *Simplicité et isolation de la première valeur propre du p-laplacien avec poids*, C. R. Acad. Sci. Paris Sér. I Math. **305** (1987), no. 16, 725–728.

[2] A. Anane and N. Tsouli, *On the second eigenvalue of the p-Laplacian*, Nonlinear partial differential equations (Fès, 1994), Pitman Res. Notes Math. Ser., vol. 343, Longman, Harlow, 1996, pp. 1–9.

[3] J. W. Barrett and W. B. Liu, *Finite element approximation of the p-Laplacian*, Math. Comp. **61** (1993), no. 204, 523–537.

[4] M. Belloni and B. Kawohl, *A direct uniqueness proof for equations involving the p-Laplace operator*, Manuscripta Math. **109** (2002), no. 2, 229–231.

[5] J. Benedikt, P. Drábek, and P. Girg, *The second eigenfunction of the p-Laplacian on the disk is not radial*, Preprint, 2010.

[6] A. Bonnet, *A deformation lemma on a C^1 manifold*, Manuscripta Math. **81** (1993), no. 3-4, 339–359.

[7] B. M. Brown and W. Reichel, *Computing eigenvalues and Fučík-spectrum of the radially symmetric p-Laplacian*, J. Comput. Appl. Math. **148** (2002), no. 1, 183–211.
[8] Y. S. Choi and P. J. McKenna, *A mountain pass method for the numerical solution of semilinear elliptic problems*, Nonlinear Anal. **20** (1993), no. 4, 417–437.
[9] M. Cuesta, D. de Figueiredo, and J.-P. Gossez, *The beginning of the Fučik spectrum for the p-Laplacian*, J. Differential Equations **159** (1999), no. 1, 212–238.
[10] E. DiBenedetto, $C^{1+\alpha}$ *local regularity of weak solutions of degenerate elliptic equations*, Nonlinear Anal. **7** (1983), no. 8, 827–850.
[11] P. Drábek and S. B. Robinson, *On the generalization of the Courant nodal domain theorem*, J. Differential Equations **181** (2002), no. 1, 58–71.
[12] J. P. García Azorero and I. Peral Alonso, *Existence and nonuniqueness for the p-Laplacian: nonlinear eigenvalues*, Comm. Partial Differential Equations **12** (1987), no. 12, 1389–1430.
[13] R. Glowinski and A. Marroco, *Sur l'approximation, par éléments finis d'ordre un, et la résolution, par pénalisation-dualité, d'une classe de problèmes de Dirichlet non linéaires*, RAIRO Analyse Numérique **9** (1975), no. R-2, 41–76.
[14] J. Horák, *Constrained mountain pass algorithm for the numerical solution of semilinear elliptic problems*, Numer. Math. **98** (2004), no. 2, 251–276.
[15] P. Juutinen and P. Lindqvist, *On the higher eigenvalues for the ∞-eigenvalue problem*, Calc. Var. Partial Differential Equations **23** (2005), no. 2, 169–192.
[16] P. Juutinen, P. Lindqvist, and J. J. Manfredi, *The ∞-eigenvalue problem*, Arch. Ration. Mech. Anal. **148** (1999), no. 2, 89–105.
[17] B. Kawohl and V. Fridman, *Isoperimetric estimates for the first eigenvalue of the p-Laplace operator and the Cheeger constant*, Comment. Math. Univ. Carolin. **44** (2003), no. 4, 659–667.
[18] B. Kawohl and T. Lachand-Robert, *Characterization of Cheeger sets for convex subsets of the plane*, Pacific J. Math. **225** (2006), no. 1, 103–118.
[19] D. Krejčiřík and A. Pratelli, *The Cheeger constant of curved strips*, arXiv:1011.3490v1, 2010.
[20] P. Lindqvist, *On the equation* $\operatorname{div}(|\nabla u|^{p-2}\nabla u) + \lambda|u|^{p-2}u = 0$, Proc. Amer. Math. Soc. **109** (1990), no. 1, 157–164.
[21] P. Lindqvist,*Addendum: "On the equation* $\operatorname{div}(|\nabla u|^{p-2}\nabla u) + \lambda|u|^{p-2}u = 0$*"*, Proc. Amer. Math. Soc. **116** (1992), no. 2, 583–584.
[22] E. Parini, *The second eigenvalue of the p-Laplacian as p goes to 1*, Int. J. Differ. Equ. (2010), Art. ID 984671, 23.
[23] M. Struwe, *Variational methods*, Springer-Verlag, Berlin, 1990.
[24] X. Yao and J. Zhou, *Numerical methods for computing nonlinear eigenpairs. I. Iso-homogeneous cases*, SIAM J. Sci. Comput. **29** (2007), no. 4, 1355–1374.

Jiří Horák
Universität zu Köln, Mathematisches Institut, 50923 Köln, Germany
E-mail address: jhorak@math.uni-koeln.de
URL: www.mi.uni-koeln.de/~jhorak/plaplace